Automated Support of Human-Induced Movements of a Swivel-Wheeled Mobile Robot

Beumer, R.M.

Award date:
2021

FACULTY OF MECHANICAL ENGINEERING
MASTER MECHANICAL ENGINEERING
CONTROL SYSTEMS TECHNOLOGY
GRADUATION PROJECT - 4ZM10

Automated Support of Human-Induced Movements of a Swivel-Wheeled Mobile Robot

CST2021.027

Author:
R.M. Beumer BSc (0967254)

Coaches:
ir. W. Houtman
dr.ir C.A. López Martínez

Supervisor:
dr.ir. M.J.G. van de Molengraft

Committee:
dr.ir. M.J.G. van de Molengraft
prof.dr. H.P.J. Bruyninckx
dr.ir. A.A.J. Lefeber
dr.ir C.A. López Martínez

Eindhoven, June 2, 2021

CONTENTS

Automated Support of Human-Induced Movements of a Swivel-Wheeled Mobile Robot

R.M. Beumer, W. Houtman, C.A. López Martínez, M.J.G. van de Molengraft

***Abstract*—Robots are more and more applied in environments shared with people, even at the level at which they physically interact. Therefore, there is a growing demand for reliable and safe robotic systems. A human can for instance execute a task in collaboration with a whole-body compliant robot. This compliant behavior can be such, that the user can safely intervene in the movement of the robot. In other applications, these robots even actively contribute to the required force to perform a movement induced by the user. This research investigates the support of human-induced movements with a mobile robot. The mobile robot employed for this project is the ropod platform, which can move using its four swivel-wheel units that consist of two actuated wheels each. The forces and torques applied to this platform by the user are estimated with a disturbance observer, which uses a - for this purpose developed - modular dynamic model of the system. Due to using this disturbance observer instead of a specific sensor, the user can apply an input anywhere on the system. Compliant behavior of the system is achieved by converting the estimated user force to an updated velocity setpoint via an admittance interface with safety constraints. This setpoint is tracked by the already existing stabilizing velocity controller for the platform. The safety constraints are partly based on the limited accuracy of the observed user input, for instance caused by the dynamic effects of the swivel-wheel units. As a consequence, some cases rather require more effort from the user than that the desired movement is supported. Modularity of the model enables the possibility to extend the approach to situations in which the wheel configuration is changed or multiple platforms collaborate. This work also proposes a general method to identify the dynamic parameters for the system in any configuration. This method is not aimed at the accuracy of the individual parameter values, but at the accuracy of the model as a whole.**

I. Introduction

The usage of robots to support humans has more and more applications. Whereas in the early days these robots usually had their own separate environment and specific task, the current developments are towards executing flexible tasks and applying them in environments shared with people as well, even until the level at which the robot and human physically interact. For instance mobile robots such as Automated Guided Vehicles (AGVs) are more and more used to automate logistics. This can be done in industrial applications, but could also be applied in other environments such as hospitals.

One of the research projects in this field is the ROPOD project, for which the goal was to create AGVs that are able to move a variety of payloads up to 1000 kg for indoor applications [1]. Each ropod (abbreviation of robotic pod) is a platform that can move using its four so-called Smart-Wheel (SWh) units. Each SWh consists of two separately actuated wheels, shown in the left picture of Fig. 1. These SWhs can swivel around the pivot points at which they are attached to the platform, as illustrated in Fig. 2. The platform base is holonomic in the horizontal plane, which means that it can translate and rotate in any direction in this plane, regardless of the orientations of the SWhs. Another important aspect of the design is the modularity as shown in Fig. 1: multiple SWhs are used for one ropod platform, and multiple platforms can form a flock of ropods that can cooperate in order to move larger objects such as hospital beds.

Supporting people in the field of logistics with robots such as ropod platforms can in some cases be done

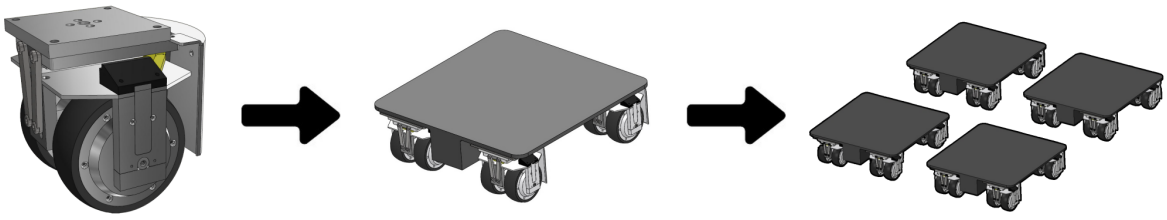

Fig. 1: Modular design concept, from left to right: Smart-Wheel, ropod platform, flock of ropods [2]

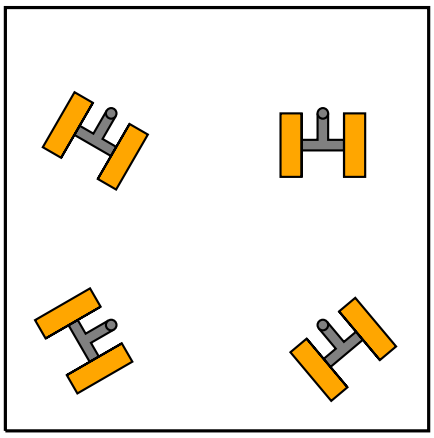

Fig. 2: Schematic top view of the ropod platform with its Smart-Wheels that can rotate around their pivot points.

autonomously, while ensuring safe interaction with people that are in the same environment. However, this research focuses on a semi-automated way to support humans when moving heavy objects, which is to let a person steer while the robot contributes to the required force to do the movements. Such an approach is very useful when for instance the task or environment is not exactly known for the robot. Besides, there could be ethical considerations that make an autonomous solution undesired, for example when moving sick beds with patients in a hospital. When the robot supports the movements, the user can move heavy objects with much less effort. This could contribute to their physical health; it has been shown that for example people whose jobs involved lifting, pulling or pushing objects of 11 kg or more have an increased risk of low back pain [3]. Furthermore, such compliant behavior of the ropods allows people to move them out of the way easily, for instance when there is an emergency. Other research projects at the Eindhoven University of Technology as a part of the ROPOD project related to compliant control have already been executed [4][5]. These projects have shown potential and hence there is a desire to continue this research.

The remainder of this work is organized as follows. In Section II, the goal of this research is explained. In Section III, other research related to this project is discussed, based on which the remaining challenges for this project follow. A more detailed description of the system used for this research is given in Section IV. In Section V, a new approach to construct a modular dynamic model of this system is presented. In Section VI, the identification of the dynamic parameters that are required for this model is explained. The control strategy that is proposed to let the robot support the human-induced movements is discussed in Section VII, followed by the experimental results in Section VIII. In Section IX the most important conclusions that can be drawn from this research and recommendations for further research are given.

II. Problem Statement

In this section, the goal of this project is explained. This project does not stand on its own, but is related to the ROPOD project. On a top level, the goal of the ROPOD project is to develop robotic pods (ropods) that are able to help humans by moving objects from one place to another and to cooperate and collaborate with each other. The focus of this research is on a semi-automated operation mode of the platform, in which the human indicates what movement the ropod should make, so that the platform can support this movement.

Examples of ways in which a user could indicate what movement of the platform is desired are for instance via a remote control device such as a joystick, or by using voice commands. However, such approaches could have a risk of giving the platform an incorrect command or be forgotten in case of an emergency. Therefore, this research focuses on a more intuitive way for the user to interact with the platform, which is via a direct physical contact by moving the system itself by hand to steer it. The platform should then deliver a part of the required power to support the human-induced motion. In this way, the user can move the platform in the same way as usual, but now by applying less force.

In the physical interaction between the robot and the human and the rest of the environment, safety is a very important aspect. Furthermore, this new project should take modularity into account, as that is one of the key aspects of the ROPOD project from a technical development and implementation point of view. Hence, the main research question for this project can be stated as:

How to design a modular and safe control strategy for supporting human-induced movements with a holonomic AGV?

The holonomic AGV this research is applied to is the ropod platform, introduced in Section I and explained in more detail in Section IV. In this context, the human-induced movements are the translations and rotation in the plane of the local surface on which the platform is. This research will be restricted to the case in which there is a single ropod platform on a horizontal surface and without a load. The desired safety and modularity of the

control strategy to be developed are descripted by the following requirements:

- *Stability of the closed loop system*
  When no external input is applied to the system, it should always control its velocity towards zero. Dangerous situations could occur when for example the ropod would continue accelerating after the user gives it a short touch and should thus be prevented.
- *Limit the speed of the platform*
  As the platform moves in an environment with humans, the desired speed limit is 5 km/h (or 1.4 m/s) [6]. Such a limit does not only help to prevent collisions, but also indirectly limits the amount of kinetic energy of the system. Depending on the mass of the platform and its load, the speed limit could be reduced.
- *Modularity and scalability of the technical solution*
  Modularity and scalability in the context of this project mean that for example it should be possible to extend the proposed solution to multiple ropods that cooperate, and that it should be flexible for an adaptation of the wheel configuration. Although this research focuses on a single ropod platform without a load, this modularity should already be considered in the design of the technical solution.

III. Related Work

In this section, the work related to this research is discussed. Based on the goal of this project and the related work, the remaining challenges become clear and the main contributions of this research are explained.

In [4], the design of a bumper that can serve as a multiple direction force sensor for the ropod platform is discussed. On each side of the platform, four forces are estimated by using distance sensors and modelling the bumper as springs and dampers. Furthermore, the work proposes a compliant control strategy called **Zone Model Predictive Control** (Z-MPC) in which the reference is replaced by a zone that is bounded by force constraints to allow compliant behavior. This approach was chosen because it can predict future states using a model of the platform as well as handle constraints, so that violation of the force constraints can be prevented.

Several approaches for force sensorless compliant control are discussed and applied to a mobile robot with omni-directional wheels in [5]. These approaches are **indirect compliance** and direct compliance, which is subdivided into **force feedback**, **impedance control** and **admittance control** and the user input is estimated by means of a disturbance observer. In short, a disturbance observer derives an estimate of the disturbance by comparing the real input to the input that would correspond to the output based on a model of the system; the difference is assumed to be caused by the disturbance. **Indirect compliance** uses the limited stiffness of a 'normal' controller that lets the robot follow a position reference. This method is not suited as a main approach for the application in this project, because it does not actively support the movements a user induces with the platform, it only allows them. **Force feedback** provides assistance for the user by magnifying their own input force. The simplicity of this method is its advantage and disadvantage at the same time: a decrease in sensed mass means a decrease in sensed damping and friction simultaneously. **Impedance control** and **admittance control** are similar to each other. For both methods, a dynamic model of the real plant and the desired plant are made. The real plant model should describe the real dynamic behavior of the system, whereas the desired plant model describes the properties of the system that would be desired by the user: for example a lower mass. The idea behind both methods is that interacting with the real plant should feel as if it is the desired plant. The way in which this is achieved, is different. In impedance control, the user input is directly translated to the control inputs that are necessary to let the platform behave as if the desired plant would receive the user input, by means of substituting the relevant terms in the equations of motion of both models into each other. In admittance control, a reference trajectory is generated based on the user input and the desired plant dynamics. Then, this trajectory is tracked by means of an inner position or velocity control loop. The control schemes of impedance control and admittance control are shown in Fig. 3 and Fig. 4 respectively.

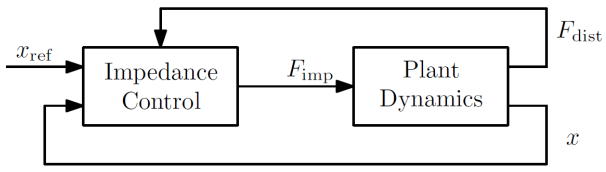

Fig. 3: Impedance control [5]

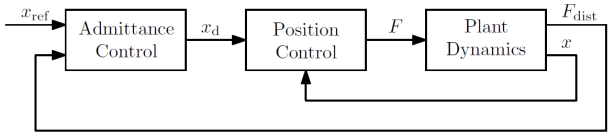

Fig. 4: Admittance control [5]

Furthermore, [7] provides an overview of publications about compliant control, subdividing them into four main categories or control concepts which are, besides

impedance control and admittance control, **hybrid force/-position control** and **parallel force/position control**. Hybrid force/position control and parallel force/position control both apply position and force control simultaneously. In hybrid force/position control, the system is split into one part that is motion-controlled and one part that is force-controlled. This is illustrated in Fig. 5, in which E is the identity matrix of size $n \times n$ and $S = \text{diag}(s_j)$, with $j = 1...n$ and n is the number of degrees of freedom. With this definition, the motion-controlled directions are indicated by $s_j = 1$ and the force-controlled directions are indicated by $s_j = 0$. In parallel force/position control, the force and motion controller can work on the same directions and the controller outputs are superimposed, as is shown in Fig. 6.

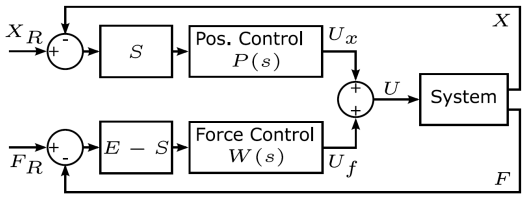

Fig. 5: Hybrid force/position control [7]

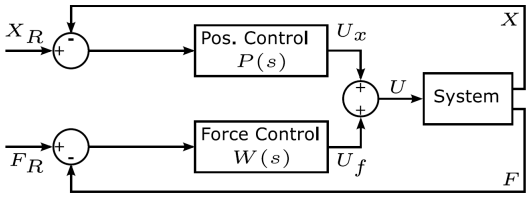

Fig. 6: Parallel force/position control [7]

A combination of different strategies is possible as well. For instance, [8] describes 'whole-body impedance control' applied to a robot that has a nonholonomic base with four wheels, with eight actuated degrees of freedom in total: one for propulsion and one for steering each wheel. The whole robot, which besides the base also consists of an upper body, is impedance controlled at the top level. Internally, the control for the upper body and the base is split, while the dynamic interaction between the two is taken into account. For the upper body, torque control is applied. For the internal control of the base an admittance interface is included, in combination with an inner velocity control loop for the actuation (steering and propulsion) of the wheels. However, the external inputs are measured by forces/torque sensors that are only present in the upper body of the robot. Therefore, the robot will not react in the desired compliant way when the external input is exerted on the mobile base.

Several miscellaneous concepts related to compliant control are:

- The concepts 'virtual caster' and 'constraint tracking' as explained in [9], where the application of those principles to a unicycle and a redundant tricycle robot are discussed. In the virtual caster mode, the robot steers in the direction of the force a user applies to it. In the constraint tracking mode, the robot only allows the user to move it in certain directions that are determined by the constraints. This principle can be useful to combine compliant behavior with safety constraints.
- A general framework for cobot control based on feedback linearization [10]. With feedback linearization, a nonlinear system is algebraically transformed into a linear system. Then, a linear controller can applied in the outer feedback loop, allowing for instance a linear analysis for the stability of the closed loop system. Proving this stability is relevant for this research, because it is one of the safety requirements stated in Section II.
- Research related to exo-skeletons, because it is an application to support movements that a human makes as well, and in which safety is very important. Examples can be found in [11], [12] and [13]. A disadvantage is that the control techniques cannot always directly be applied to the ropod platform, as for example in [12] the human is supposed to be part of the closed loop and the system would be unstable without the human.

Many of the mentioned concepts use a dynamic model of the system. Multiple methods exist to model a multibody system in which the different components physically interact with each other. The two most commonly used approaches to construct such a dynamic model are the Newton-Euler method and the Euler-Lagrange method, both explained in [14] and [15]. Although both approaches can be applied to describe the exact same dynamics, their different methods of analysis provide different insights regarding the desired modularity and scalability. Furthermore, dynamic models contain dynamic parameters such as the masses of components, for which the values should be identified. Detailed information about dynamic parameter identification is for instance given in [14], [16] and [17], which provides an overview of offline and online identification methods.

Contributions

In most of the described related works, a specific end-effector such as a force/torque sensor is used to measure the user input. However, in some cases it might be difficult or inconvenient for a user to reach for those

sensors, as a load could for instance be attached above the platform. Besides, in accordance with the requirement to set up the control strategy in a modular way, it would be desired for the user to be able to exert his force anywhere on the system, which could be on the load as well. Therefore, in the proposed solution of this research the user input will not be measured by a specific end-effector, but means of a disturbance observer, similar to [5]. The application of a disturbance observer requires a dynamic model of the complete system in order to be able to detect a user input anywhere on the system. One of the main differences with the robot used in [5] is the fact that the dynamics of the ropod platform are more complex, making the application of a disturbance observer more challenging but still worth to explore because of the explained advantages. In combination with the goal to have a modular and scalable solution, this makes constructing a modular and scalable dynamic model one of the main contributions of this work.

The modularity and scalability of this model are achieved by exploiting the recursive structure of the Newton-Euler method to describe the dynamics. This is done in such a way, that it yields a modular expression and closed form solution for the direct equations of motion that relate the wheel inputs and user input to the movement of the central component. For the application in this research, the central component is the platform base. When the method would be extended to multiple platforms and a load, the load can be the central component as well.

In addition, this work proposes a method to identify the dynamic parameters based on [16], but set up in such a way that it provides the flexibility of being used to identify the parameters for the modular model in general. I.e.: the same method can be applied for all different compositions of the modular system.

Furthermore, the level of accuracy of the estimated user input by the disturbance observer is an important factor for the choice of the applied control strategy, in particular considering the required safety. The proposed control strategy is based on admittance control with additional constraints within the admittance interface in order to meet the safety requirements stated in Section II. This is done by choosing the constraints based on the following objectives:

- If the user does not exert a force on the platform, any observed input should not be taken into account. Otherwise, there is a risk of entering a positive feedback loop, leading to unstable behavior of the system.
- If a user input is observed, the direction should be correct. Cases in which the platform would react as if it is pushed or pulled in a completely different direction than the user does, can of course be dangerous and should therefore be avoided.
- The generated velocity setpoint by the admittance interface is restricted so that the velocity limit will not be exceeded.

IV. System Description

The system used for this research is the ropod platform, introduced in Section I. Here, a more detailed description of this system is given.

The ropod, shown in the middle picture of Fig. 1, is a wheeled platform of approximately 0.65 m $\times$ 0.65 m, and has a height of maximum 0.15 m for the initial protoype and 0.10 m for the final product [2]. As described in Section I, the platform can move using its four Smart-Wheel (SWh) units that can swivel around the pivot points at which they are attached to the platform base. Each SWh consists of two separately actuated wheels, that are connected to the SWh frame via a mechanism that has an internal degree of freedom, illustrated in Fig. 7. This mechanism enables both wheels to be in contact with the ground without being statically overdetermined. The SWh frame, so the SWh without the individual wheels, will in this research also be called the wheel hub, in order to make a distinction between this part only and the SWh as a whole.

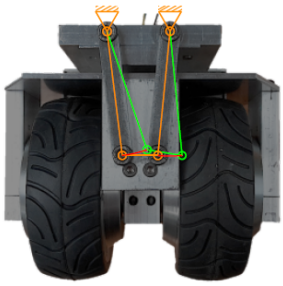

Fig. 7: Internal DOF of a Smart-Wheel [18]

Two SWhs are directly attached to the platform base, whereas the two others are connected via an intermediate beam that is attached to the bottom of the base with a hinge as depicted in Fig. 8. This hinge allows the beam to rotate around the horizontal axis perpendicular to the beam. Hence, the base of the platform is in fact supported at three points, which make it statically determined in the vertical direction and the two rotations about the axes that span the horizontal plane.

An important property of the SWhs is their caster offset as shown in Fig. 9: there is a distance s_w between (1)

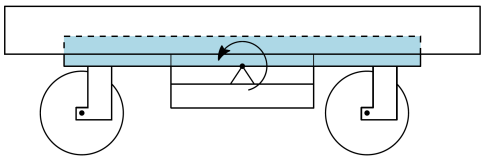

Fig. 8: Schematic side view of the ropod with the hinged beam indicated in blue [18]

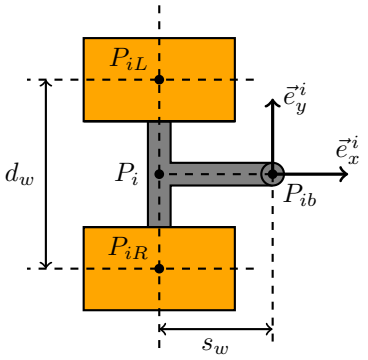

Fig. 9: Schematic top view of a Smart-Wheel in which s_w is the caster offset.

the vertical axis through point P_{ib} around which a SWh rotates with respect to the base and (2) the wheel axles through points P_{iL} and P_{iR}. The platform can drive in the direction the SWh is oriented towards ($\vec{e}_x^{\,i}$) by letting the wheels rotate in the same direction. A movement perpendicular to this direction can be performed by letting the two wheels rotate in opposite directions. The point P_{ib} at which the SWh is attached to the base will then rotate around the center P_i of two wheels and thus move in the direction of $\vec{e}_y^{\,i}$. By superimposing these two movements, the point at which the SWh is attached to the base can move in any direction. Because this holds for each point at which a SWh is attached, the platform base can rotate and translate in any direction in the horizontal plane and is therefore holonomic. Another consequence of the caster offset is that some movements of the platform will require the wheel units to rotate around their pivot axes in order to make the transition from their unstable 'pulling' configuration to stable 'pushing' configuration.

V. Modular Dynamic Model

In this section, the derivation of the modular dynamic model of the platform described in Section IV is explained. The model contains all movements in the horizontal plane (two translations and one rotation) of the platform base, the wheel hubs and the individual wheels and additionally the rotation of the individual wheels about their axis of rolling movement. The fact that the model is constructed in a modular and scalable way, makes it possible to be flexible for changing the wheel configuration (amount and locations of SWhs), cope with a malfunctioning wheel or extend the approach for cases in which multiple platforms collaborate.

Assumptions

The platform is a multibody system in which the different components interact with each other due to their physical connections that are modeled as kinematic constraints. Besides the internal interaction forces, the platform interacts with the ground via its wheels. This interaction with the ground is modeled by imposing kinematic constraints on the wheels. An important assumption made by using those kinematic constraints is that there is no wheel slip, neither longitudinal or lateral. A solution to prevent excessive wheel slip with this platform has been investigated in [18] and is based on imposing bounds on the wheel input torques. Furthermore, this research restricts itself to movements of the platform on flat and horizontal surfaces only, justifying two other assumptions:

- The internal degrees of freedom explained in Section IV, which are meant to allow all wheels to be in contact with the ground in a statically determined way, are not explicitly included in the model as degrees of freedom. The assumption that implicitly takes the consequences into account in the model are that it is assumed that the geometric parameters are constant while all wheels remain in contact with the ground. Contact of the wheels with the ground is also crucial for the controllability [19] of the system.
- Gravity has no direct influence in the plane of movement. The indirect influence it has on the movement by having an effect on the friction parameters is implicitly included in those, as will be discussed in Appendix D.

Method

As pointed out in Section III, the different methods of analysis of the Newton-Euler method and the Euler-Lagrange method provide different insights regarding the desired modularity and scalability. Within the Euler-Lagrange formulation, modularity could be achieved by adding the contribution of a new component to the total Lagrangian of the system and formulating the new kinematic constraints that are imposed on the new component. These constraints can then be taken into account in the equations of motion by adding Lagrange multipliers, which act as additional constraint forces in the equations of motion in order to meet the constraint equations. However, in this way the amount of equations

of motion and constraints will increase with the number of components. Furthermore, for this platform type, all kinematics are (indirectly) related to each other so that the computations become extensive very soon, in particular when multiple platforms would be connected to each other. Hence, in this way good scalability is not achieved. The Newton-Euler approach, on the other hand, leads to a set of equations whose structure allows a recursive type of solution, in which the physical modularity of the ropod platform can be recognized more intuitively. In the remainder of this section, the proposed way to exploit this recursive structure in order do derive a modular and scalable dynamic model of the system is explained. The main idea behind the approach is that (a) the platform base is seen as the central component to which all other components are directly or indirectly attached and that (b) the kinematic constraints that each added SWh introduces can directly be used to substitute the constrained variables, so that the equations of motion that remain will directly describe the relation between the wheel inputs, the user input and the movement of the platform base. Therefore, in Section V-A first the dynamic model of the platform base is given, already including the possible forces at the points at which the SWhs are attached. Then, the kinematic model based on the geometry of the platform's structure is discussed in Section V-B. Subsequently, the dynamic model of a SWh is explained in Section V-C. Then, the way in which the kinematics are used to combine the dynamics of all components into the equations of motion that directly describe the relation between the wheel inputs and the platform base movement is elaborated in Section V-D. The resulting expressions for the forward and inverse dynamics are described in Section V-E.

Since the main goal of this section is to explain the structure of the modular dynamic model, the influence of friction is for the sake of simplicity omitted in this section and is discussed separately in Appendix D. There it is also shown how the modeled friction can be included in this structure. The values of the geometric parameters of the ropod platform used for this research can be found in Appendix A. The values of the dynamic parameters are determined experimentally, as will be explained in Section VI.

Notation convention

The notation that will be used for all coordinates in this section is $r^a_{A_1/A_2} = \begin{bmatrix} x^a_{A_1/A_2} & y^a_{A_1/A_2} \end{bmatrix}^\top$ to represent the coordinates of point P_{A_1} with respect the origin, expressed in the directions $\vec{e}^a_x$ and $\vec{e}^a_y$ of frame a. The same convention is used for their first and second time derivatives $\dot{r}^a_{A_1} = \begin{bmatrix} \dot{x}^a_{A_1} & \dot{y}^a_{A_1} \end{bmatrix}^\top$ and $\ddot{r}^a_{A_1} = \begin{bmatrix} \ddot{x}^a_{A_1} & \ddot{y}^a_{A_1} \end{bmatrix}^\top$. When using $r^a_{A_1/A_2}$, so with with an additional point P_{A_2}, the coordinates of point A_1 are given with respect to this point A_2. Furthermore, the short notations s_{θ_b} and c_{θ_b} will be used for respectively $\sin(\theta_b)$ and $\cos(\theta_b)$ and similarly this will be done for the sine and cosine of θ_i and δ_i.

A. Platform Base Model

The platform base is seen as the central component to which all other components are attached directly or indirectly. The three degrees of freedom (DOFs) of this base are $q^0_b = \begin{bmatrix} x^0_b & y^0_b & \theta_b \end{bmatrix}^\top$. It should be noted that the use of global coordinates is in fact not necessary for this project, as the same results could be achieved by only using the local platform frame of reference. However, the choice has been made to use the global coordinates for practical reason related to implementation in the existing software and simulation and debugging purposes. The movements in these directions are influenced by the forces and torques that act on the platform base, resulting from the other components, the environment and the user. The other components are the wheel hubs and individual wheels (via the wheels hubs) and the load. For now, the forces from the user, environment and load are combined into $F_b = \begin{bmatrix} F_{bx} & F_{by} & T_{bz} \end{bmatrix}^\top$, representing respectively the forces in the local x- and y-direction (through the center of mass) and the torque about the vertical axis of the platform base. The interaction forces with the wheel hubs at their pivot points are denoted by $F_{ixy} = \begin{bmatrix} F_{ix} & F_{iy} \end{bmatrix}^\top$ for $i \in \{1, ..., n\}$ with n the number of SWhs. These are expressed in the local x- and y-direction of the platform base as well. A schematic overview of this platform base model with all forces and torques exerted on it is shown in Fig. 10. The equations of motions of the platform base are then given by:

$$M_b \ddot{q}^0_b = B_{F_b} F_b + \sum_{i=1}^{n} B_{F_{ixy}} F_{ixy} \tag{1}$$

in which M_b is the mass matrix of only the platform base itself:

$$M_b = \begin{bmatrix} m_b & 0 & 0 \\ 0 & m_b & 0 \\ 0 & 0 & J_{zz,b} \end{bmatrix} \tag{2}$$

The matrices B_{F_b} and $B_{F_{ixy}}$ convert the forces expressed in local coordinates to their contributions to the global directions:

$$B_{F_b} = \begin{bmatrix} c_{\theta_b} & -s_{\theta_b} & 0 \\ s_{\theta_b} & c_{\theta_b} & 0 \\ 0 & 0 & 1 \end{bmatrix} \tag{3}$$

$$B_{F_{ixy}} = \begin{bmatrix} c_{\theta_b} & -s_{\theta_b} \\ s_{\theta_b} & c_{\theta_b} \\ -y^b_{ib/b} & x^b_{ib/b} \end{bmatrix} \tag{4}$$

in which $x^b_{ib/b}$ and $y^b_{ib/b}$ represent the local coordinates of the point P_{ib} at which SWh i is attached to the base.

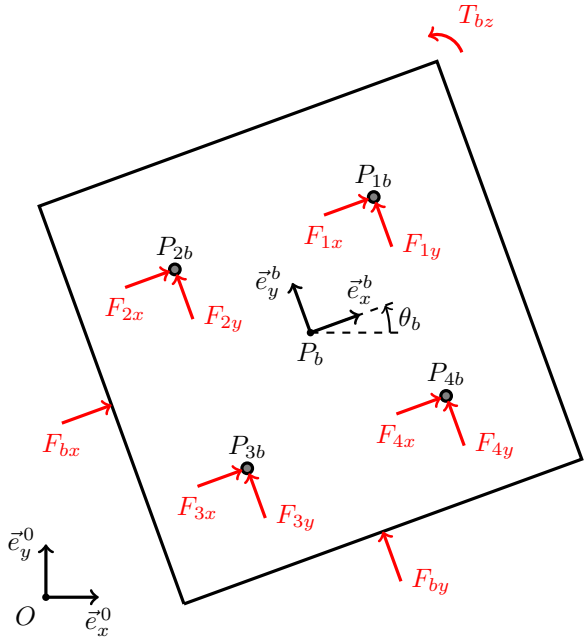

Fig. 10: Schematic overview of the dynamic model of the platform base with the attachment points of the Smart-Wheels. All forces and torques that work on the base are indicated in red.

B. Kinematics

A schematic overview of a SWh is given in Fig. 11. The angle δ_i defines the orientation of SWh i with respect to the platform base. As the dimensions of the SWh are known and using the assumption of no slip, a given movement of the base directly determines the movement of the SWh. The coordinates of the pivot point location P_{ib} of SWh i are:

$$\underbrace{\begin{bmatrix} x^0_{ib} \\ y^0_{ib} \end{bmatrix}}_{r^0_{ib}} = \underbrace{\begin{bmatrix} x^0_b \\ y^0_b \end{bmatrix}}_{r^0_b} + \underbrace{\begin{bmatrix} c_{\theta_b} & -s_{\theta_b} \\ s_{\theta_b} & c_{\theta_b} \end{bmatrix}}_{R^0_b} \underbrace{\begin{bmatrix} x^b_{ib/b} \\ y^b_{ib/b} \end{bmatrix}}_{r^b_{ib/b}} \tag{5a}$$

in which $r^b_{ib/b}$ is constant, as it is a body-fixed vector expressed in the frame of the body itself. The velocity and acceleration of this point are calculated by taking respectively the first and second time derivatives of (5a):

$$\dot{r}^0_{ib} = \dot{r}^0_b + \underbrace{\begin{bmatrix} -\dot{\theta}_b s_{\theta_b} & -\dot{\theta}_b c_{\theta_b} \\ \dot{\theta}_b c_{\theta_b} & -\dot{\theta}_b s_{\theta_b} \end{bmatrix}}_{\dot{R}^0_b} r^b_{ib/b} \tag{5b}$$

$$\ddot{r}^0_{ib} = \ddot{r}^0_b + \underbrace{\begin{bmatrix} -\ddot{\theta}_b s_{\theta_b} - \dot{\theta}^2_b c_{\theta_b} & -\ddot{\theta}_b c_{\theta_b} + \dot{\theta}^2_b s_{\theta_b} \\ \ddot{\theta}_b c_{\theta_b} - \dot{\theta}^2_b s_{\theta_b} & -\ddot{\theta}_b s_{\theta_b} - \dot{\theta}^2_b c_{\theta_b} \end{bmatrix}}_{\ddot{R}^0_b} r^b_{ib/b} \tag{5c}$$

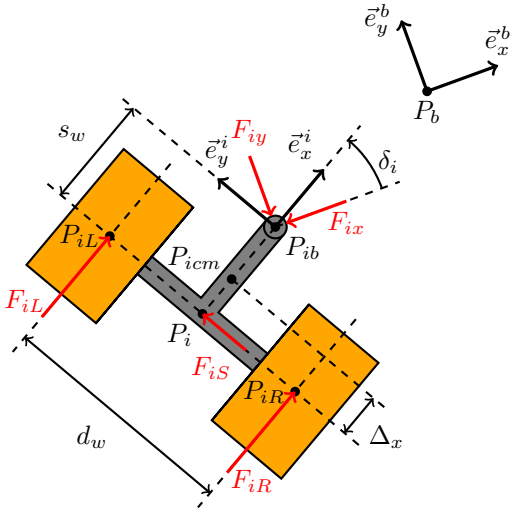

Fig. 11: Schematic top view of a Smart-Wheel and the modeled forces that work on the wheel hub indicated in red

The kinematic center P_i of SWh i is defined as the point at which the lines through the individual wheel axes and the line trough the pivot point P_{ib} would intersect perpendicular in the horizontal plane. Its coordinates are given by:

$$\underbrace{\begin{bmatrix} x^0_i \\ y^0_i \end{bmatrix}}_{r^0_i} = \underbrace{\begin{bmatrix} x^0_{ib} \\ y^0_{ib} \end{bmatrix}}_{r^0_{ib}} + \underbrace{\begin{bmatrix} c_{\theta_i} & -s_{\theta_i} \\ s_{\theta_i} & c_{\theta_i} \end{bmatrix}}_{R^0_i} \underbrace{\begin{bmatrix} -s_w \\ 0 \end{bmatrix}}_{r^i_{i/ib}} \tag{6a}$$

in which $\theta_i = \theta_b + \delta_i$ and s_w is the caster offset. Taking into consideration that $r^i_{i/ib}$ is constant, the velocity and acceleration are calculated by taking the time derivatives:

$$\dot{r}^0_i = \dot{r}^0_{ib} + \underbrace{\begin{bmatrix} -\dot{\theta}_i s_{\theta_i} & -\dot{\theta}_i c_{\theta_i} \\ \dot{\theta}_i c_{\theta_i} & -\dot{\theta}_i s_{\theta_i} \end{bmatrix}}_{\dot{R}^0_i} r^i_{i/ib} \tag{6b}$$

$$\ddot{r}_i^0 = \ddot{r}_{ib}^0 + \underbrace{\begin{bmatrix} -\ddot{\theta}_i s_{\theta_i} - \dot{\theta}_i^2 c_{\theta_i} & -\ddot{\theta}_i c_{\theta_i} + \dot{\theta}_i^2 s_{\theta_i} \\ \ddot{\theta}_i c_{\theta_i} - \dot{\theta}_i^2 s_{\theta_i} & -\ddot{\theta}_i s_{\theta_i} - \dot{\theta}_i^2 c_{\theta_i} \end{bmatrix}}_{\ddot{R}_i^0} r_{i/ib}^i \tag{6c}$$

for which $\dot{\theta}_i$ and $\ddot{\theta}_i$ follow from the assumption that the wheels do not slip sideways, which means that the movement of the kinematic center P_i can not be sideways with respect to the SWh orientation as well. Mathematically, this nonholonomic constraint means that the projection of the velocity $\dot{r}_i^0$ of this point on the local sideward direction is zero:

$$-s_{\theta_i}\dot{x}_i^0 + c_{\theta_i}\dot{y}_i^0 = 0 \tag{7}$$

After substituting the expressions for $\dot{x}_i^0$ and $\dot{y}_i^0$ from (5b) and (6b) into (7), the resulting equation can be rewritten to:

$$\dot{\theta}_i = \frac{1}{s_w}\left(-s_{\theta_i}\dot{x}_b^0 + c_{\theta_i}\dot{y}_b^0 + \dot{\theta}_b\left(x_{ib/b}^b c_{\delta_i} + y_{ib/b}^b s_{\delta_i}\right)\right) \tag{8a}$$

Taking the time derivative of this expression yields the angular acceleration:

$$\begin{aligned}\ddot{\theta}_i = \frac{1}{s_w}\Big(&-c_{\theta_i}\dot{\theta}_i\dot{x}_b^0 - s_{\theta_i}\ddot{x}_b^0 - s_{\theta_i}\dot{\theta}_i\dot{y}_b^0 + c_{\theta_i}\ddot{y}_b^0 \\ &+ \ddot{\theta}_b\left(x_{ib/b}^b c_{\delta_i} + y_{ib/b}^b s_{\delta_i}\right) \\ &+\dot{\theta}_b\left(-x_{ib/b}^b s_{\delta_i}\dot{\delta}_i + y_{ib/b}^b c_{\delta_i}\dot{\delta}_i\right)\Big)\end{aligned} \tag{8b}$$

Similar to r_i^0 and its first and second time derivatives, the position r_{icm}^0 and its time derivatives are given by:

$$r_{icm}^0 = r_{ib}^0 + R_i^0 r_{icm/ib}^i \tag{9a}$$

$$\dot{r}_{icm}^0 = \dot{r}_{ib}^0 + \dot{R}_i^0 r_{icm/ib}^i \tag{9b}$$

$$\ddot{r}_{icm}^0 = \ddot{r}_{ib}^0 + \ddot{R}_i^0 r_{icm/ib}^i \tag{9c}$$

in which, assuming symmetry of the SWhs and a constant distance Δ_x between the kinematic center and the center of mass of a SWh, $r_{icm/ib}^i = \begin{bmatrix} -s_{cm} & 0 \end{bmatrix}^\top$ with $s_{cm} = s_w - \Delta_x$.

Similarly as well, the positions of the centers of the individual wheels, and their derivatives, are determined by:

$$r_{iw}^0 = r_{ib}^0 + R_i^0 r_{iw/ib}^i \tag{10a}$$

$$\dot{r}_{iw}^0 = \dot{r}_{ib}^0 + \dot{R}_i^0 r_{iw/ib}^i \tag{10b}$$

$$\ddot{r}_{iw}^0 = \ddot{r}_{ib}^0 + \ddot{R}_i^0 r_{iw/ib}^i \tag{10c}$$

in which subscript $w \in \{L, R\}$ represents either the left wheel or the right wheel, $r_{iL/ib}^i = \begin{bmatrix} -s_w & \frac{d_w}{2} \end{bmatrix}^\top$ and $r_{iR/ib}^i = \begin{bmatrix} -s_w & \frac{-d_w}{2} \end{bmatrix}^\top$.

Schematic overviews regarding the rolling movement of both the left and the right wheel including the sign conventions for the wheel angle ϕ_{iw} are shown in Fig. 12. Due to the assumption that there is no slip in longitudinal direction of the wheel as well, the local forward velocity of the point P_{iw} is directly coupled to the rotational velocity $\dot{\phi}_{iw}$ of the wheel:

$$R_w\dot{\phi}_{iw} = c_{\theta_i}\dot{x}_{iw}^0 + s_{\theta_i}\dot{y}_{iw}^0 \tag{11}$$

in which R_w is the wheel radius. Hence, dividing by R_w and taking the derivative with respect to time yields the angular acceleration of the wheel:

$$\ddot{\phi}_{iw} = \frac{1}{R_w}\left(-s_{\theta_i}\dot{\theta}_i\dot{x}_{iw}^0 + c_{\theta_i}\ddot{x}_{iw}^0 + c_{\theta_i}\dot{\theta}_i\dot{y}_{iw}^0 + s_{\theta_i}\ddot{y}_{iw}^0\right) \tag{12}$$

C. Wheel Dynamics

1) Individual Wheels

The dynamics of the individual wheels are split into two parts: one part of the directions of movement in which the individual wheels can be considered to be rigidly attached to the wheel hub and one part for the movement directions in which it should be treated separately. This split is made based on the assumption that the center of mass of the wheel is on its axis of rotation (for the rolling movement) and that this axis is fixed with respect to the wheel hub. Hence, the translations and rotation of the individual wheel in the horizontal plane are included in the wheel hub dynamics. The only relevant remaining movement is the rotation about its axis of rolling, which is analyzed here. Schematic overviews regarding the dynamics for both the left and the right wheel are provided in Fig. 12. The relevant torque and forces for this motion are the wheel input torque τ_{iw}, the reaction force from the ground in longitudinal direction F_{igw} and the interaction force with the wheel hub F_{iw}.

The most intuitive way to derive the equation is to first include the mass m_w of the individual wheel in this model and then set it equal to 0. In the local longitudinal direction $\vec{e}_x^i$, the acceleration is determined by the interaction force with the wheel hub and the reaction force from the ground:

$$m_w\ddot{x}_{iw}^i = -F_{iw} + F_{igw} \tag{13}$$

Since the interaction force with the wheel hub has no arm with respect to the wheel axle, the angular acceleration

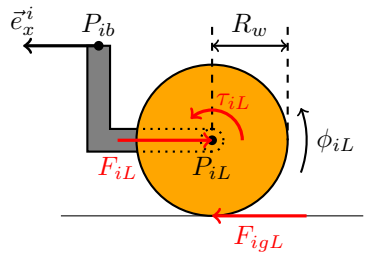

(a) Left wheel

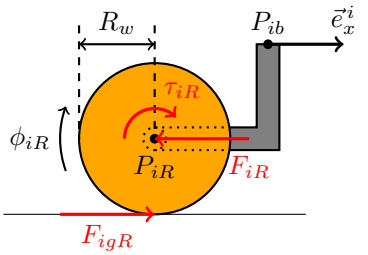

(b) Right wheel

Fig. 12: Schematic side views of the individual wheels and the modeled forces and torques that work on them indicated in red

is determined by the wheel input torque and the reaction force from the ground:

$$J_{rot,w}\ddot{\phi}_{iw} = \tau_{iw} - F_{igw}R_w \tag{14}$$

However, the rolling and translational accelerations are coupled when no slip is assumed: $\ddot{x}^i_{iw} = R_w\ddot{\phi}_{iw}$. Substituting this into (13) and solving for F_{igw} yields:

$$F_{igw} = m_w R_w \ddot{\phi}_{iw} + F_{iw} \tag{15}$$

This can be substituted in (14) to get:

$$J_{rot,w}\ddot{\phi}_{iw} = \tau_{iw} - \left(m_w R_w \ddot{\phi}_{iw} + F_{iw}\right) R_w \tag{16}$$

which, after setting the individual wheel mass for this part of the model equal to zero, results in:

$$\ddot{\phi}_{iw} = \frac{1}{J_{rot,w}} \left(\tau_{iw} - F_{iw}R_w\right) \tag{17}$$

Note that the interaction force computed in this way is different than the interaction force that would be computed if the mass of the individual wheel was not taken as zero for this part. As the mass will be contained in the dynamics of the wheel hub, this does not have an influence on the dynamics described by the model as a whole. Therefore, this difference is only relevant when the value of this specific interaction should be known.

2) Wheel Hubs

For each wheel hub, the forces considered are the interaction forces F_{iL} and F_{iR} with both wheels in local longitudinal direction, the sum F_{iS} of the lateral interaction forces with the wheels (as they work along the same axis) and the interaction forces F_{ix} and F_{iy} with the platform base in the two horizontal directions, as shown in Fig. 11. Then, the equations of motion for the wheel hub are:

$$M_{wh} \underbrace{\begin{bmatrix} \ddot{x}^0_{icm} \\ \ddot{y}^0_{icm} \\ \ddot{\theta}_i \end{bmatrix}}_{\ddot{q}^0_{icm}} = A_{iwh} \begin{bmatrix} F_{ix} \\ F_{iy} \\ F_{iS} \end{bmatrix} + A_{iwh2} \underbrace{\begin{bmatrix} F_{iL} \\ F_{iR} \end{bmatrix}}_{F_{iLR}} \tag{18}$$

in which

$$M_{wh} = \begin{bmatrix} m_{wh} & 0 & 0 \\ 0 & m_{wh} & 0 \\ 0 & 0 & J_{wh,zz} \end{bmatrix} \tag{19}$$

$$A_{iwh} = \begin{bmatrix} -c_{\theta_b} & s_{\theta_b} & -s_{\theta_i} \\ -s_{\theta_b} & -c_{\theta_b} & c_{\theta_i} \\ s_{cm}s_{\delta_i} & -s_{cm}c_{\delta_i} & -\Delta_x \end{bmatrix} \tag{20}$$

$$A_{iwh2} = \begin{bmatrix} c_{\theta_i} & c_{\theta_i} \\ s_{\theta_i} & s_{\theta_i} \\ -\frac{d_w}{2} & \frac{d_w}{2} \end{bmatrix} \tag{21}$$

in which m_{wh} is the mass of the wheel hub including the masses of the individual wheels attached to it, as explained in the Section V-C1. Similarly, $J_{wh,zz}$ is the moment of inertia about the vertical axis trough the center of mass of the wheel hub including the individual wheels.

D. Total Platform Dynamics

After combining the equations of motion of all components, together with the constraints that follow from the kinematic model, a solvable system of equations remains.

A method has been found to reduce the system of equations to a form in which the relation between wheel inputs and platform base accelerations can be described directly, by means of eliminating all additional variables with a step-by-step approach. These additional variables are the interaction forces and intermediate coordinates, velocities and accelerations. Besides (and due to) the fact that this omits the need of a solver, it complies with the desired modularity and scalability of the model.

The main idea of the method is to replace these additional variables by a linear combination of other variables until only the desired reduced set of second order derivatives and forces/torques remain. All lower order derivatives and platform configuration constants can be used in the

parametrization coefficients, as they are all known or can directly be calculated, measured or estimated. The notation for parametrization that will be used throughout this explanation is $z_0 = a_{z_1}^{z_0} z_1 + a_{z_2}^{z_0} z_2 + ... + a_{z_m}^{z_0} z_m + b^{z_0}$ in order to parametrize z_0 in terms of z_1 to z_m, where $a_{z_1}^{z_0}$ to $a_{z_m}^{z_0}$ and b^{z_0} are the parametrization coefficients. In case these coefficients are matrices, which is dependent on the dimensions of the variables, they will be denoted by capitals.

The starting point for constructing the reduced set of equations of motion is (1), because it describes the motion of the platform base. The only variables in this equation that should be eliminated are the interaction forces with the wheel hubs $F_{ixy} = \begin{bmatrix} F_{ix} & F_{iy} \end{bmatrix}^\top$. As $\det(A_{iwh}) = -s_w \neq 0$, A_{iwh} is invertible and hence a closed form parametric expression for the interaction forces and the sideward force can be derived using the equations of motions of the wheel hubs from (18). This is achieved by rewriting them to a new form in which the parametrizations of $\ddot{q}_{icm}^0$ and F_{iLR}, which will be explained in the remainder of this section, are already used:

$$\begin{aligned}
\begin{bmatrix} F_{ix} \\ F_{iy} \\ F_{iS} \end{bmatrix} &= \underbrace{A_{iwh}^{-1} M_{wh}}_{A_{\ddot{q}_{icm}^0}^{F_{ixyS}}} \ddot{q}_{icm}^0 + \underbrace{-A_{iwh}^{-1} A_{iwh2}}_{A_{F_{iLR}}^{F_{ixyS}}} F_{iLR} \\
&= A_{\ddot{q}_{icm}^0}^{F_{ixyS}} \underbrace{\left(A_{\ddot{q}_b^0}^{\ddot{q}_{icm}^0} \ddot{q}_b^0 + b^{\ddot{q}_{icm}^0} \right)}_{\ddot{q}_{icm}^0} \\
&\quad + A_{F_{iLR}}^{F_{ixyS}} \underbrace{\left(A_{\ddot{q}_b^0}^{F_{iLR}} \ddot{q}_b^0 + A_{\tau_i}^{F_{iLR}} \tau_i + b^{F_{iLR}} \right)}_{F_{iLR}} \\
&= \underbrace{\left(A_{\ddot{q}_{icm}^0}^{F_{ixyS}} A_{\ddot{q}_b^0}^{\ddot{q}_{icm}^0} + A_{F_{iLR}}^{F_{ixyS}} A_{\ddot{q}_b^0}^{F_{iLR}} \right)}_{A_{\ddot{q}_b^0}^{F_{ixyS}}} \ddot{q}_b^0 \\
&\quad + \underbrace{A_{F_{iLR}}^{F_{ixyS}} A_{\tau_i}^{F_{iLR}}}_{A_{\tau_i}^{F_{ixyS}}} \tau_i + \underbrace{A_{\ddot{q}_{icm}^0}^{F_{ixyS}} b^{\ddot{q}_{icm}^0} + A_{F_{iLR}}^{F_{ixyS}} b^{F_{iLR}}}_{b^{F_{ixyS}}}
\end{aligned} \tag{22}$$

The parametrization of $\ddot{q}_{icm}^0$ can be written as:

$$\underbrace{\begin{bmatrix} \ddot{r}_{icm}^0 \\ \ddot{\theta}_{icm} \end{bmatrix}}_{\ddot{q}_{icm}^0} = \underbrace{\begin{bmatrix} A_{\ddot{q}_b^0}^{\ddot{r}_{icm}^0} \\ a_{\ddot{q}_b^0}^{\ddot{\theta}_{icm}} \end{bmatrix}}_{A_{\ddot{q}_b^0}^{\ddot{q}_{icm}^0}} \ddot{q}_b^0 + \underbrace{\begin{bmatrix} b^{\ddot{r}_{icm}^0} \\ b^{\ddot{\theta}_{icm}} \end{bmatrix}}_{b^{\ddot{q}_{icm}^0}} \tag{23}$$

for which the separate parametrizations of $\ddot{r}_{icm}^0$ and $\ddot{\theta}_i$. are obtained as follows. In order to parametrize $\ddot{\theta}_i$, (8b) is rewritten to the form:

$$\ddot{\theta}_i = a_{\ddot{q}_b^0}^{\ddot{\theta}_i} \ddot{q}_b^0 + b^{\ddot{\theta}_i} \tag{24}$$

with

$$a_{\ddot{q}_b^0}^{\ddot{\theta}_i} = \frac{1}{s_w} \begin{bmatrix} -s_{\theta_i} \\ c_{\theta_i} \\ x_{ib/b}^b c_{\delta_i} + y_{ib/b}^b s_{\delta_i} \end{bmatrix}^\top \tag{25}$$

and

$$\begin{aligned}
b^{\ddot{\theta}_i} = \frac{1}{s_w} \Big(& -c_{\theta_i} \dot{\theta}_i \dot{x}_b^0 - s_{\theta_i} \dot{\theta}_i \dot{y}_b^0 \\
& + \dot{\theta}_b \left(-x_{ib/b}^b s_{\delta_i} \dot{\delta}_i + y_{ib/b}^b c_{\delta_i} \dot{\delta}_i \right) \Big)
\end{aligned} \tag{26}$$

The parametrization of $\ddot{r}_{icm}^0$ is more elaborate, mainly because a parametrization for the second time derivative of the rotation matrix is required in order to apply a systematic (modular) approach. The details of the proposed method to do this matrix parametrization are explained in Appendix B. Starting from (9c), the parametrization of $\ddot{r}_{icm}^0$ can now be written as follows:

$$\begin{aligned}
\ddot{r}_{icm}^0 &= \ddot{r}_{ib}^0 + \ddot{R}_i^0 r_{icm/ib}^i \\
&= \left(A_{\ddot{q}_b^0}^{\ddot{r}_{ib}^0} \ddot{q}_b^0 + b^{\ddot{r}_{ib}^0} \right) + \left(A_{\ddot{q}_b^0}^{\ddot{R}_i^0 r_{icm/ib}^i} \ddot{q}_b^0 + b^{\ddot{R}_i^0 r_{icm/b}^{ib}} \right) \\
&= \underbrace{\left(A_{\ddot{q}_b^0}^{\ddot{r}_{ib}^0} + A_{\ddot{q}_b^0}^{\ddot{R}_i^0 r_{icm/ib}^i} \right)}_{A_{\ddot{q}_b^0}^{\ddot{r}_{icm}^0}} \ddot{q}_b^0 + \underbrace{b^{\ddot{r}_{ib}^0} + b^{\ddot{R}_i^0 r_{icm/b}^{ib}}}_{b^{\ddot{r}_{icm}^0}}
\end{aligned} \tag{27}$$

for which $A_{\ddot{q}_b^0}^{\ddot{R}_i^0 r_{icm/ib}^i}$ and $b^{\ddot{R}_i^0 r_{icm/b}^{ib}}$ are calculated according to the approach explained in Appendix B, and $A_{\ddot{q}_b^0}^{\ddot{r}_{ib}^0}$ and $b^{\ddot{r}_{ib}^0}$ follow from the parametrization of $\ddot{r}_{ib}^0$ which follows the same approach as this parametrization. That parametrization of $\ddot{r}_{ib}^0$ is based on (5c) and requires the straightforward parametrization of $\ddot{r}_b^0$:

$$\ddot{r}_b^0 = \begin{bmatrix} \ddot{x}_b^0 \\ \ddot{y}_b^0 \end{bmatrix} = \underbrace{\begin{bmatrix} 1 & 0 & 0 \\ 0 & 1 & 0 \end{bmatrix}}_{A_{\ddot{q}_b^0}^{\ddot{r}_b^0}} \ddot{q}_b^0 + \underbrace{\begin{bmatrix} 0 \\ 0 \end{bmatrix}}_{b^{\ddot{r}_b^0}} \tag{28}$$

What remains is the parametrization of F_{iLR} with respect to $\tau_i = \begin{bmatrix} \tau_{iL} & \tau_{iR} \end{bmatrix}^\top$ and $\ddot{q}_b^0$. Using (17) we have:

$$\begin{aligned}
F_{iw} &= \frac{1}{R_w} \left(\tau_{iw} - J_{rot,w} \ddot{\phi}_{iw} \right) \\
&= \underbrace{-\frac{J_{rot,w}}{R_w}}_{a_{\ddot{\phi}_{iw}}^{F_{iw}}} \ddot{\phi}_{iw} + \underbrace{\frac{1}{R_w}}_{a_{\tau_{iw}}^{F_{iw}}} \tau_{iw} \\
&= a_{\ddot{\phi}_{iw}}^{F_{iw}} \underbrace{\left(a_{\ddot{q}_b^0}^{\ddot{\phi}_{iw}} \ddot{q}_b^0 + b^{\ddot{\phi}_{iw}} \right)}_{\ddot{\phi}_{iw}} + a_{\tau_{iw}}^{F_{iw}} \tau_{iw} \\
&= \underbrace{a_{\ddot{\phi}_{iw}}^{F_{iw}} a_{\ddot{q}_b^0}^{\ddot{\phi}_{iw}}}_{a_{\ddot{q}_b^0}^{F_{iw}}} \ddot{q}_b^0 + \underbrace{a_{\ddot{\phi}_{iw}}^{F_{iw}} b^{\ddot{\phi}_{iw}}}_{b^{F_{iw}}} + a_{\tau_{iw}}^{F_{iw}} \tau_{iw}
\end{aligned} \tag{29}$$

for which $a^{\ddot{\phi}_{iw}}_{\ddot{q}_b^0}$ and $b^{\ddot{\phi}_{iw}}$ follow from the parametrization of $\ddot{\phi}_{iw}$ using (12):

$$\begin{aligned}
\ddot{\phi}_{iw} &= \frac{1}{R_w}\left(-s_{\theta_i}\dot{\theta}_i\dot{x}^0_{iw} + c_{\theta_i}\ddot{x}^0_{iw} + c_{\theta_i}\dot{\theta}_i\dot{y}^0_{iw} + s_{\theta_i}\ddot{y}^0_{iw}\right) \\
&= \underbrace{\begin{bmatrix}\frac{1}{R_w}c_{\theta_i} & \frac{1}{R_w}s_{\theta_i}\end{bmatrix}}_{a^{\ddot{\phi}_{iw}}_{\ddot{r}^0_{iw}}}\underbrace{\begin{bmatrix}\ddot{x}^0_{iw}\\ \ddot{y}^0_{iw}\end{bmatrix}}_{\ddot{r}^0_{iw}} + \frac{1}{R_w}\left(-s_{\theta_i}\dot{\theta}_i\dot{x}^0_{iw} + c_{\theta_i}\dot{\theta}_i\dot{y}^0_{iw}\right) \\
&= a^{\ddot{\phi}_{iw}}_{\ddot{r}^0_{iw}}\underbrace{\left(A^{\ddot{r}^0_{iw}}_{\ddot{q}_b^0}\ddot{q}_b^0 + b^{\ddot{r}^0_{iw}}\right)}_{\ddot{r}^0_{iw}} + \frac{1}{R_w}\left(-s_{\theta_i}\dot{\theta}_i\dot{x}^0_{iw} + c_{\theta_i}\dot{\theta}_i\dot{y}^0_{iw}\right) \\
&= \underbrace{a^{\ddot{\phi}_{iw}}_{\ddot{r}^0_{iw}}A^{\ddot{r}^0_{iw}}_{\ddot{q}_b^0}}_{a^{\ddot{\phi}_{iw}}_{\ddot{q}_b^0}}\ddot{q}_b^0 + \underbrace{a^{\ddot{\phi}_{iw}}_{\ddot{r}^0_{iw}}b^{\ddot{r}^0_{iw}} + \frac{1}{R_w}\left(-s_{\theta_i}\dot{\theta}_i\dot{x}^0_{iw} + c_{\theta_i}\dot{\theta}_i\dot{y}^0_{iw}\right)}_{b^{\ddot{\phi}_{iw}}}
\end{aligned} \tag{30}$$

for which $A^{\ddot{r}^0_{iw}}_{\ddot{q}_b^0}$ and $b^{\ddot{r}^0_{iw}}$ follow from the parametrization of $\ddot{r}^0_{iw}$, which follows exactly the same approach as the parametrization of $\ddot{r}^0_{icm}$, but now using (10c) as a starting point; the only difference is that the body-fixed vector has different values.

By combining (29) for both $w \in \{L, R\}$, the parametrization of the column F_{iLR} can be written as:

$$\underbrace{\begin{bmatrix}F_{iL}\\ F_{iR}\end{bmatrix}}_{F_{iLR}} = \underbrace{\begin{bmatrix}a^{F_{iL}}_{\ddot{q}_b^0}\\ a^{F_{iR}}_{\ddot{q}_b^0}\end{bmatrix}}_{A^{F_{iLR}}_{\ddot{q}_b^0}}\ddot{q}_b^0 + \underbrace{\begin{bmatrix}a^{F_{iL}}_{\tau_{iL}} & 0\\ 0 & a^{F_{iR}}_{\tau_{iR}}\end{bmatrix}}_{A^{F_{iLR}}_{\tau_i}}\underbrace{\begin{bmatrix}\tau_{iL}\\ \tau_{iR}\end{bmatrix}}_{\tau_i} + \underbrace{\begin{bmatrix}b^{F_{iL}}\\ b^{F_{iR}}\end{bmatrix}}_{b^{F_{iLR}}} \tag{31}$$

Now the whole parametrization has been finished, the resulting equations of motion can be analyzed. Substituting the result of (22) in (1) yields:

$$\begin{aligned}
M_b\ddot{q}_b^0 &= B_{F_b}F_b + \sum_{i=1}^{n} B_{F_{ixy}}\underbrace{\left(A^{F_{ixy}}_{\ddot{q}_b^0}\ddot{q}_b^0 + A^{F_{ixy}}_{\tau_i}\tau_i + b^{F_{ixy}}\right)}_{F_{ixy}} \\
\underbrace{\left(M_b - \sum_{i=1}^{n} B_{F_{ixy}}A^{F_{ixy}}_{\ddot{q}_b^0}\right)}_{M_{dir}}\ddot{q}_b^0 &= B_{F_b}F_b \\
&\quad + \sum_{i=1}^{n}\underbrace{B_{F_{ixy}}A^{F_{ixy}}_{\tau_i}}_{B_{\tau_i}}\tau_i + \underbrace{\sum_{i=1}^{n} B_{F_{ixy}}b^{F_{ixy}}}_{b_{dir}} \\
M_{dir}\ddot{q}_b^0 &= B_{F_b}F_b + \underbrace{\begin{bmatrix}B_{\tau_1} & B_{\tau_2} & \cdots & B_{\tau_n}\end{bmatrix}}_{B_\tau}\underbrace{\begin{bmatrix}\tau_1\\ \tau_2\\ \vdots\\ \tau_n\end{bmatrix}}_{\tau} + b_{dir} \\
M_{dir}\ddot{q}_b^0 &= B_{F_b}F_b + B_\tau\tau + b_{dir}
\end{aligned} \tag{32}$$

in which $A^{F_{ixy}}_{\ddot{q}_b^0}$ represents the first two rows of $A^{F_{ixyS}}_{\ddot{q}_b^0}$, $A^{F_{ixy}}_{\tau_i}$ represents the first two rows of $A^{F_{ixyS}}_{\tau_i}$ and $b^{F_{ixy}}$ represents the first two elements of $b^{F_{ixyS}}$.

E. Forward and Inverse Dynamics

The direct equations of motion can be rewritten in different forms to enable several applications. For instance, the forward dynamics have been used for simulation purposes, and could also be applied in various types of model based control. As M_{dir} is a 3×3 matrix, a parametric version of a closed form expression for its inverse could even be calculated. An analysis of the invertibility of this matrix is given in Appendix C, in which is shown that M_{dir} is invertible under the sufficient condition that m_b, $J_{zz,b}$, m_{wh}, $J_{zz,wh}$ and $J_{rot,w}$ are positive and R_w, s_w and d_w are nonzero. This condition is met by the modular components of which the platform consists. The forward dynamics can now be described by:

$$\ddot{q}_b^0 = M_{dir}^{-1}\left(B_{F_b}F_b + B_\tau\tau + b_{dir}\right) \tag{33}$$

When the number of SWhs n is 2 or larger, which will in general be the case, the system is over-actuated because the number of inputs ($2n$) will be more than the number of DOFs (3). The solution to the inverse dynamics is then non-unique, which allows a certain custom distribution of the inputs. For instance, the sum of the squares of the inputs can be minimized by using the pseudo-inverse B_τ^+ of the input matrix:

$$\tau_{minRMS} = B_\tau^+\left(M_{dir}\ddot{q}_b^0 - B_{F_b}F_b - b_{dir}\right) \tag{34}$$

More elaborate torque distribution algorithms are possible as well. For instance, the platform could actively cope with the effects of a detected malfunctioning SWh by setting the torques of the corresponding individual wheels to zero and distribute the torque over the other wheels only. Furthermore, a constrained optimization could be performed in order to include torque bounds to prevent excessive wheel slip, as discussed in the beginning of this section where the assumptions were explained.

VI. Dynamic Parameter Identification

The values of the dynamic parameters are crucial for the accuracy of the model. In this research, an offline identification method similar to the one applied in [16] is used and will be explained in this section, followed by the results.

A. Main Method

The equations of motion (EOM) from (32) can be rewritten in a form in which the dynamic parameters m_b, $J_{zz,b}$, m_{wh}, $J_{zz,wh}$ and $J_{rot,w}$ are isolated:

$$\begin{aligned}
M_{dir}\ddot{q}_b^0 &= \underbrace{B_{F_p}F_p + B_\tau\tau}_{b_{ID}} + b_{dir} \\
M_{dir}\ddot{q}_b^0 - b_{dir} &= b_{ID} \\
A_{ID}\underline{m} &= b_{ID}
\end{aligned} \tag{35}$$

in which $\underline{m} = \begin{bmatrix} m_b & J_{zz,b} & m_{wh} & J_{zz,wh} & J_{rot,w} \end{bmatrix}^\top$ and A_{ID} is a 3×5 matrix and computed such that $A_{ID}\underline{m} = M_{dir}\ddot{q}_b^0 - b_{dir}$, which is possible by using the structure of the modular model. The elaboration of how to do this in a modular and systematic way is very similar to how the direct dynamic model is constructed in Section V. In fact, now all parametrization steps are taken towards eliminating all variables that are not the dynamic parameters. This method can be extended to the model in which friction is added, as explained in Appendix D-C, and yields the system of equations:

$$A_{ID,ext}\underline{m}_{ext} = b_{ID} \tag{36}$$

in which $\underline{m}_{ext}$ also contains the friction coefficients. It should be noted that $A_{ID,ext} = A_{ID,ext}(q_b^0, \dot{q}_b^0, \ddot{q}_b^0, \delta_1, ..., \delta_n)$ and $b_{ID} = b_{ID}(q_b^0, \dot{q}_b^0, \delta_1, ..., \delta_n, \tau)$. Hence, q_b^0 and its time derivatives, δ_i for $i \in \{1, ...n\}$ and τ should be known, calculated, measured or estimated in order to find the values for $A_{ID,ext}$ and b_{ID}. The method to acquire this data is discussed in Section VI-B. The data is acquired for multiple combinations of the state and input variables, in order to form a stacked version of the system of the equations from (36):

$$\underbrace{\begin{bmatrix} A_{ID,ext,1} \\ A_{ID,ext,2} \\ \vdots \\ A_{ID,ext,n_d} \end{bmatrix}}_{A_{ID,ext,tot}} \underline{m}_{ext} = \underbrace{\begin{bmatrix} b_{ID,1} \\ b_{ID,2} \\ \vdots \\ b_{ID,n_d} \end{bmatrix}}_{b_{ID,tot}} \tag{37}$$

in which n_d is the number of data combinations for which the equations are stacked. In general, as the model will not be perfect and the data will contain some measurement noise, this stacked system of $3n_d$ equations cannot be solved perfectly for $\underline{m}_{ext}$. The solution $\underline{m}^*_{ext}$ that gives the least squares error can be found by using the pseudo-inverse:

$$\underline{m}^*_{ext} = A^+_{ID,ext,tot} b_{ID,ext,tot} \tag{38}$$

In this way, this method provides a general way to estimate any dynamic parameter in the model and it will map the inputs and outputs of the rewritten direct EOM as accurate as possible (in the sense of least squares) for the given measurement data. The latter is the most important when using the direct dynamic model as a whole only. In general, this method does not give the most accurate values for the individual dynamic parameters. When a individual component of the model would be of interest, for instance for debugging purposes, more specific identification methods such as measuring the masses of components with a scale can be more accurate and reliable and might thus be preferred. Considering the desired modularity and scalability for this research, the generality of the proposed method is an important advantage. Besides, the equation errors of the direct EOM are directly related to the observed disturbance as will be explained in Section VII-B. As one of the objectives is that no user disturbance should be observed when it is not present, it is more important to make this error as small as possible than to have the most accurate values for the individual parameters. For these reasons, the proposed method is selected.

Excitation Trajectory

Now, a trajectory for the platform should be chosen such that all relevant dynamics are excited. No user input F_b is applied during these experiments, so that it can be filled in as zero in the EOM. The trajectory is tracked by the existing velocity controller for the ropod platform [2]. The choice has been made to apply a 'typical trajectory', which contains straights, corners, rotations, constant velocity and acceleration. Such a trajectory was preferred over a general method to generate an identification trajectory based on the dynamic model as described in [16], as the physical experimental environment brings some restrictions to the trajectories that can be followed and because some dynamic effects are not desired to be included and because. The most important of these effects is the transition of the wheels from their unstable 'pulling' to their stable 'pushing' configuration, which often causes severe vibrations of the platform and sometimes some wheel slip. The achieved accuracy of the fit of the model for these effects was significantly worse than required in order to be useful and at the same time it had a negative influence on the accuracy of the fit for the other parts. Therefore, these effects have been omitted in the identification trajectory and another solution has been found to cope with the major inaccuracies in those regimes, as will be explained in Section VII.

A weighting has been applied for the rotational EOM in order to scale the magnitude with the translation, as due to the different unit it appeared to be significantly lower for the applied trajectory and hence not weighted enough to receive a good fit otherwise. This weighting is chosen such, that the mean squares of the entries of $b_{ID,tot}$ that belong to the EOM for rotation θ_b, is equal to the mean squares for the entries of $b_{ID,tot}$ that belong to the EOM for the translations. Furthermore, in order to avoid a bias for a certain direction, the same experiment has been repeated with a mirrored version of the trajectory, i.e. all right corners were replaced by left corners and vice versa. Besides, the experiment has been repeated with the original trajectory with a minus sign for each translation

and rotation, and a mirrored version of this trajectory as well. Then, the four resulting weighted stacked systems of equations are again stacked to form one large stacked system of equations. This large system of equations is used to find the dynamic parameter values $\underline{m}^*_{ext}$ that gives the least squares error as explained.

B. Data Acquisition and Filtering

As discussed in Section VI-A, the required data for the dynamic parameter estimation are the platform pose q_b^0 and its time derivatives, the pivot angles δ_i for $i \in \{1, ..., n\}$ and the wheel input torques τ. Once these variables are known, all other variables can be calculated using the relations in Section V. The wheel inputs are calculated by multiplying the measured motor currents with the known motor torque constant. The pivot angles δ_i and individual wheel angles ϕ_{iw} for $i \in \{1, ..., n\}$ and $w \in \{L, R\}$ are measured by encoders. These values are, using the kinematic model of the platform, converted to updated measurement values for the pose q_b^0 of the platform, which is defined to be zero at the initialization. As the data can be filtered offline and afterwards, non-causal filters such as zero-phase low pass filters can be applied in order to improve the accuracy of the method. For this purpose, an approach similar to the one explained in [16] has been applied. I.e., velocities and acceleration are calculated by central differencing and the Matlab function `smooth` is applied to filter the data. The main difference is that within this function we use the method 'loess' (LOcal polynomial regrESSion), whereas in [16], the method 'rloess' (Robust LOESS) is applied. In the robust variant, there is an additional step to assign lower weights to outliers in the regression. However, this addition significantly increased the computation time while no significant effect was found in the output.

C. Results

The experimental results of the dynamic parameter identification are depicted in Fig. 13. For each of the three degrees of freedom of the rewritten form of the direct EOM in (36), it shows the model fit $A_{ID,ext}\underline{m}^*_{ext}$ in red compared to the filtered data b_{ID} in blue, with the error in yellow. The fit is based on the combination of the four variants of the typical trajectory together, but the results are in this figure only shown for the original trajectory. The numerical values found for the dynamic parameters using this method are given in Table II in Appendix E. The residual RMS errors over the four trajectories combined are 7.03 N for the translations and 1.62 Nm for the rotation.

Although a low error at the level of the direct EOM is the most important for this research, the fact that

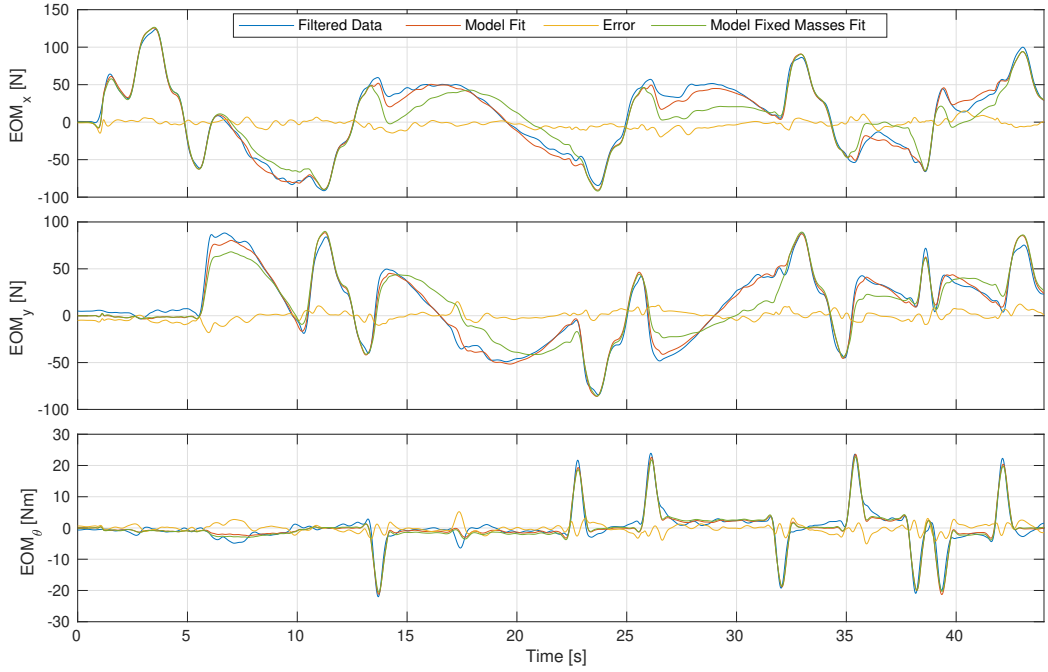

Fig. 13: Results of the model fit (orange) on the filtered data (blue) and its error (yellow) for the dynamic parameter identification experiment. The model fit with fixed mass values is shown in green.

for instance the identified mass values were negative indicates that some dynamic effects might be missing in the model. As the applied method fits all parameters at once, they can be used to correct for such missing effects and thus get an unrealistic value in order to improve the overall accuracy of the model. So, despite the individual parameter values being less relevant than the overall accuracy for this research, it is relevant to investigate the effect that causes these negative mass values. For that purpose, all geometric parameters were verified, the zero positions of the pivot angles were checked and influence of the location of the center of gravity of the platform base was investigated. However, none of these factors solved the issue. Then, the masses of the platform base and SWhs were measured so that their correct values could be fixed for the model fit. The model fit with those fixed masses is shown in green in Fig. 13 and the resulting numerical values for the parameters can be found in Table II in Appendix E as well. It can be seen that this fit is significantly less accurate than the fit for which all parameters are free, the RMS errors are respectively 12.41 N and 1.68 Nm for the translations and rotation. Therefore, the numerical values of the original fit are, despite the negative mass values, used for the remainder of this research. It should be noted that the sufficient condition that the inertial parameters should be positive for the direct mass matrix to be invertible is not met with these values. However, this does not yield any limitations for the implementation in this research, as the inverse is not required for the proposed control strategy that will be discussed in Section VII.

Another remark worth mentioning for the specific platform used for this research is the symmetric distribution of the SWhs. Data from simulations in which the model is perfect and no noise or disturbances is present, showed that $A_{ID,ext,tot}$ loses its full rank when the SWhs are attached to the platform base at symmetric positions P_{ib}, independent of the pivot angels. This effect was not present when adjusting one of the attachment locations. Although the data from the real system does contain noise and the matrix $A_{ID,ext,tot}$ can be full rank, a singular value decomposition shows that the matrix is ill-conditioned, which has a negative influence on the accuracy of the individual parameters. Again, as the main interest is on the accuracy at the level of the direct EOM, this is not a problem for this specific research.

VII. Control Strategy

The control strategy is the way in which the user input is converted to the wheel inputs in order to support the movements the user induces on the platform. As described in Section III, several approaches exist to achieve such compliant control. The strategy chosen for this research is based on admittance control, as this offers an appropriate way to combine the desired compliant properties of the platform with the objectives related to safety as stated in Section III. In this section, the choice for this framework is further explained, followed by the details of the implementation. Experimental results are given in Section VIII.

Impedance control, which is similar to admittance control, was the selected strategy in [5]. The difference between those strategies is that in impedance control there is no velocity setpoint and velocity controller, but the control is directly done on a force level. This difference is an advantage and disadvantage at the same time for this project. The advantage is that a human user does not think in terms of exact velocities that should be achieved, and an interaction with the platform based on forces is more intuitive. However, as in this strategy the wheel inputs are purely calculated using the dynamic model and estimated user input, this would require a very accurate model and estimation of the applied user force in order to achieve a good performance and stability at the same time. Although this gives good results in simulations in which the simulated system is the same as the model, the model appeared to be not accurate enough to let it work in a safe way on the physical platform. Hence, for this research a different strategy based on admittance control is proposed, in which the admittance interface that generates a velocity setpoint is also used to incorporate additional safety constraints.

In this approach, the user input is estimated by a disturbance observer and can thus be applied anywhere on the platform. A schematic overview of the strategy is given in Fig. 14. The approach can be split in four parts. First, the state variables are estimated. Then, the user input can be estimated by the disturbance observer using the wheel inputs, state variables and the dynamic model. Next, the estimated user input is translated to an updated velocity setpoint that the platform should follow. Finally, this velocity setpoint is tracked by a velocity controller. In this section, these four parts are discussed in more detail one by one, followed by a demonstration of all components working together to achieve compliant behavior of the platform.

A. State Estimation

The state estimates, as well as all other required variables, are acquired similar to the approach described in Section VI-B. The platform base pose measurement is for instance still based on the wheel and pivot encoder data and the kinematic model. The main difference is that for the real-time implementation, the non-causal filtering

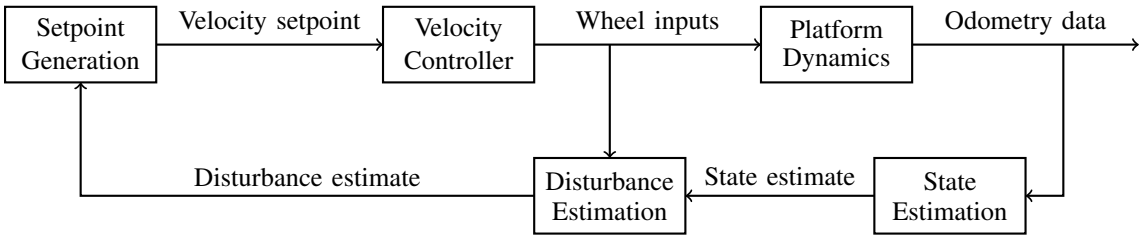

Fig. 14: Schematic overview of the proposed control strategy

using the `smooth` function and central differencing can not be applied to compute the derivatives. Instead, a Kalman filter is applied to do those estimations based on the pose measurements and a double integrator model for each DOF of the platform base.

B. Disturbance Observer

The dynamic model can be used to construct an estimate $\hat{F}_b$ for the user input F_b. The estimator relies on the fact that (32) can be rewritten to:

$$F_b = B_{F_b}^{-1}\left(M_{dir}\ddot{q}_b^0 - B_\tau \tau - b_{dir}\right) \tag{39}$$

which can be done because B_{F_b} is invertible, as $\det(B_{F_b}) = 1$ according to its expression in (3). For the model in which friction is included, the same can be done based on (65) from Appendix D:

$$F_b = B_{F_b}^{-1}\left(M_{dir}\ddot{q}_b^0 - B_\tau\left(\tau + \tau_{fw}\right) - B_{\tau_{fp}}\tau_{fp} - b_{dir}\right) \tag{40}$$

for which all terms on the right side are filled in using the estimated state variables and input torques. A low-pass filter with a 10 Hz bandwidth is applied to the resulting signal to yield the user input estimate $\hat{F}_b$. The bandwidth is chosen based on a balance between the suppression of high frequent noise and a typical human reaction time [20].

As explained in Section VI, the dynamic parameters have been chosen such, that the equation errors of the EOM were minimized while there was no user input. These errors directly correspond to the calculation of the user input estimate, as can be seen in (40), and are only separated by a rotation from the global to local frame by $B_{F_b}^{-1}$. In this way, the chosen method contributes to the objective of not observing a user input when there is none. The other objective related to the disturbance observer is that when a user input is observed, it should be observed in the correct direction. Experiments that have been executed in order to test whether the designed disturbance observer contributes to this objective as well, are discussed in Section VIII-A.

C. Velocity Setpoint Generation

The velocity setpoint generator serves as an admittance interface between the observed disturbance and the velocity controller. Besides, it contains additional constraints in order to meet the objectives related to safety. The generated setpoint is a velocity setpoint based on a desired acceleration that follows from the state and the observed disturbance. This desired acceleration is determined using the desired dynamics of the platform, that are described by:

$$M_{des}\ddot{q}_b^0 + D_{des}\dot{q}_b^0 = B_{F_b}F_b \tag{41}$$

with M_{des} and D_{des} diagonal matrices with the desired inertial and damping parameters on their diagonal. Those desired values represent that dynamic properties of the system as the user would experience when interacting with the platform via his input F_b. In theory, this would make it possible for the user to interact with the system without feeling the dynamics of the SWhs and the large mass of the platform itself. The desired mass and inertia can be chosen freely in order to have more or less support from the platform for the movements that the user intends to make with it. However it is recommended to base them on the accuracy of the observed disturbance, as the settings influence how sensitive the platform reacts to the user input and the estimation error that it contains. The chosen values for this project are a desired mass $m_{des} = 20$ kg and a desired moment of inertia $J_{des} = 2.5$ kgm^2. The desired damping can be chosen freely as well. In general, more damping increases robustness, while it makes moving the platform heavier. A guideline for choosing the value is the desired exponential decay rate of the velocity setpoint when no observed disturbance would be present. In this project, the value has been chosen such, that the velocity setpoint would halve every second.

We can rewrite (41) to:

$$\ddot{q}_b^0 = M_{des}^{-1}\left(-D_{des}\dot{q}_b^0 + B_{F_b}F_b\right) \tag{42}$$

in order to yield the desired acceleration that can be used to update the velocity setpoint accordingly. However, instead of doing this directly by filling in the estimates

for $\dot{q}_b^0$ and F_b, we apply some constraints related to the safety objectives from Section III:

- The observed disturbance is only used starting from a limit value, to meet the objective that no disturbance should be taken into account when the user does not apply an input. An indication for the force and torque limit values can be derived from the RMS errors of the model fit in the dynamic parameter identification in Section VI. First, the applied limits were taken as three times the RMS errors for the translation and rotation, but in practice these values were not safe enough yet. The chosen values that did meet the objective of not reacting to non-present user inputs were found to be 40 N and 10 Nm.
- The observed disturbance is not taken into account at all when at least one of the pivot angle velocities $\dot{\delta}_i$ exceeds 1.5 rad/s. This value is chosen based on a typical level for which the limit would be exceeded when the wheels flip, because we know that the model is very inaccurate in those cases, as explained in Section VI.
- The setpoint velocity and acceleration are limited to 1 m/s and 1 m/s^2 for the translation and 1 rad/s and 1 rad/s^2 for the rotation. These limits are chosen because at higher levels, in particular during corners, the observed disturbance was significantly less accurate than otherwise and could lead to unstable behavior. This velocity limit is stricter than the desired speed limit of 1.4 m/s for safety, which is thus met in this way.

D. Velocity Controller

The used controller is the already existing and stabilizing velocity controller including a torque distribution algorithm for the ropod platform, as explained in [2]. It should be noted that this controller is not optimized for the purpose it is used for in this project. For example, the integration action of the applied velocity controller should not be too strong when using it for compliant control, to prevent the system from reacting too strong to a built-up error after the user intuitively expects that the system will not react anymore. However, from experiments such as the one described in Section VIII-B it can be concluded that the controller suffices and is not a limiting factor to achieve the goal of this project.

VIII. Experimental Results

To test the performance of the proposed control strategy, several experiments have been executed. In this section, first the experiments to test the disturbance observer without the application of compliant control will be discussed. Then, the results of an experiment to demonstrate the combination of all components of the control strategy working together are shown. In the discussion of the results, the objectives as stated in Section III are considered as well.

A. Disturbance Observer Experiments

In order to test whether the designed disturbance observer does observe users input in the correct direction, an experiment has been executed in which the platform followed a straight path while it was pushed three times from different directions. A schematic overview of these three applied forces is given in Fig. 15. One force was applied in longitudinal direction, one in lateral direction and one force off-centered in order to exert a torque with respect to the platform center as well. The observed disturbance during this experiment is shown in Fig. 16, in which the peaks that correspond to the applied user inputs are clearly visible and start around $t = 3$ s, $t = 6$ s and $t = 9$ s. As the observed disturbance is expressed in the local frame of reference, the directions of the peaks correctly correspond to the directions in which the forces were applied. Also the torque peak during the third applied force is observed in the correct clockwise direction. So although the ground truth of the location, direction and magnitudes of the user inputs applied in this experiment are not known exactly, it does give a good indication that the directions are observed correctly, in correspondence with the objective.

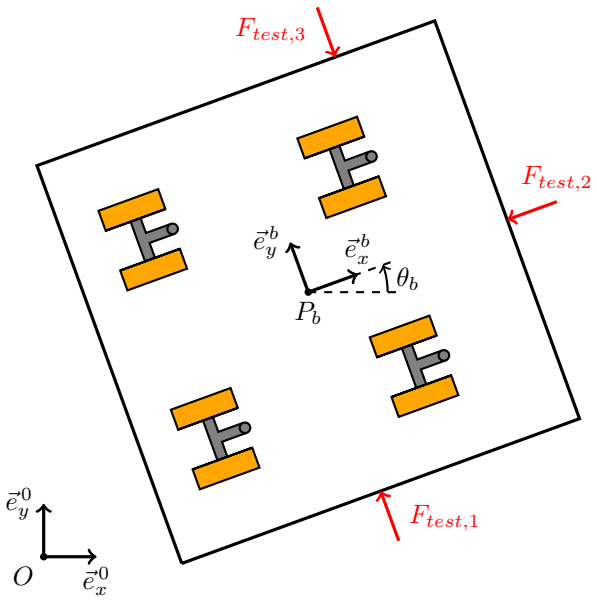

Fig. 15: Schematic overview of the exerted user inputs (in red) on the platform to test the disturbance observer.

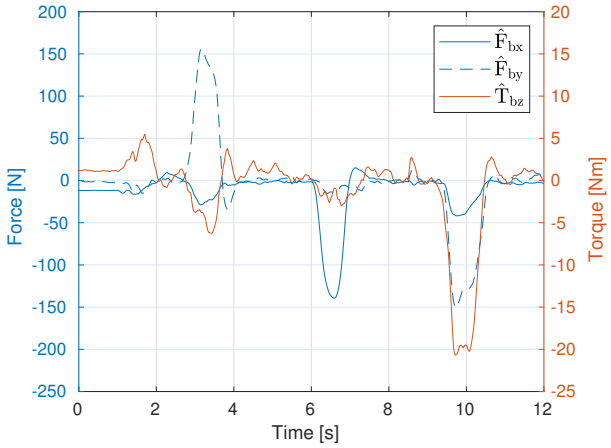

Fig. 16: Observed disturbance by the platform when being pushed from different sides while following a straight trajectory.

Another experiment has been executed in order to get an indication of the accuracy of the magnitude of the estimated user input as well. For this experiment, a setup with a hanging mass of 10 kg, connected to the platform via pulleys was used. The setup is shown in Fig. 17. Given the gravity constant g being 9.81 m/s^2, this should cause a disturbance of about 98 ± 15 N on the platform. The uncertainty boundaries are based on the identified friction of about 10 N due to the pulleys and the small vertical acceleration levels of the mass, which were 0.5 m/s^2 or lower during the experiments.

As well dynamic as static experiments have been executed using this setup, for which the range of the observed disturbance was from 80 N to 170 N, all in the correct direction. In general, the inaccuracy of the observed disturbance was larger when the wheels were aligned perpendicular to the exerted force than when the wheels were aligned in the same direction as the exerted force. In particular the static experiments allow for an analysis for the cause of the inaccuracies, as the values of the identified dynamic parameters do not have any influence on the observed disturbance as long as the estimated velocities and accelerations are zero. The only factors that do play a role in those cases are the wheel input torques, static friction and the geometric configuration of the platform. The hypothesis is that the inaccuracy of the observed disturbance is thus caused by the static friction, in particular for the rolling movement of the wheels. This effect is, according to the dynamic model, magnified by a factor $\frac{d_w}{2s_w}$ on platform level when the alignment of the wheels is perpendicular compared to the situation in which they are aligned parallel to the exerted force. This

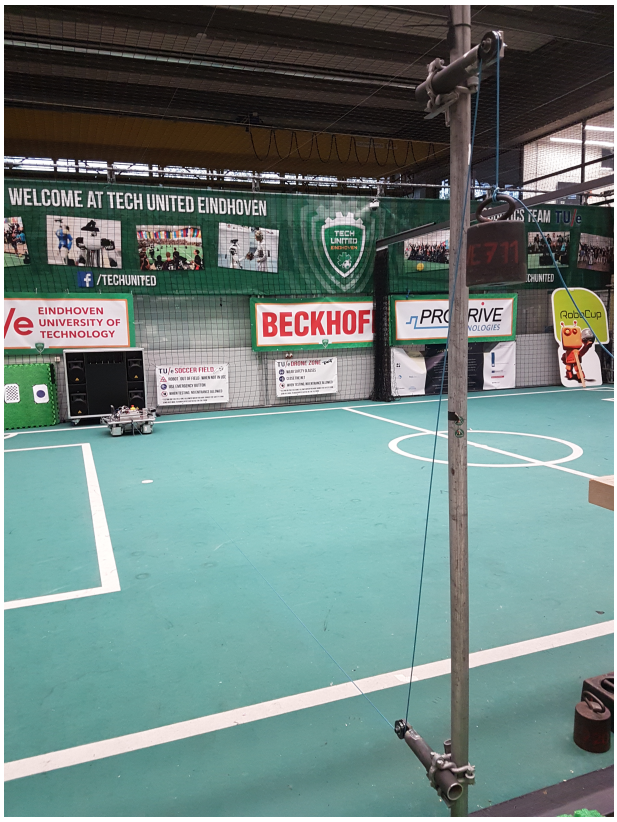

Fig. 17: Setup of experiments with a hanging mass connected to the platform with a rope via pulleys.

magnification factor is 4 for the geometric parameters of the used platform, as can be found in Appendix A. The hypothesis is supported by similar results from an experiment that was done in order to eliminate the role of the wheel input torques. The control of the platform was herein turned off so that all inputs were zero. Then, the force exerted by the hanging 10 kg mass was more than enough to let the platform accelerate from standstill when the wheels were aligned in the same direction, but was not enough to start a movement of the platform when the wheels were aligned in perpendicular direction. This also means that a user should provide a very large force before it could be observed in such situations in which the wheels are not aligned. According to the hypotheses, this effect could be strongly diminished by increasing the caster offset s_w, which has not been done in this project but certainly is recommended for further research. Besides, this adaption would help to prevent caster flutter, as explained in [21].

B. Compliant Control Demonstration

To demonstrate the combination of all components of the control strategy, an experiment was executed in which

the platform was pushed from standstill so that it began accelerating and was then pushed again from the other side to stop its movement. The results of this experiment are shown in Fig. 18, in which can be seen that as soon as the observed user force exceeds the limit of 40 N around $t = 1$ s, the generated velocity setpoint and estimated velocity start increasing until around $t = 2$ s when the force is not applied anymore. Then, due to the artificial damping, the velocity setpoint and the estimated velocity show an exponential decrease as long as no force is applied. Lastly between $t = 4$ s and $t = 5$ s, the platform also reacts as desired to the force that is applied in the end to stop its movement. The experiment also shows that at the start the velocity setpoint restricts itself by the maximum acceleration of 1 m/s^2 as desired, even though the applied force would be enough to cause a larger acceleration. It can be seen that the force applied to stop the movement is much smaller but already sufficient as well.

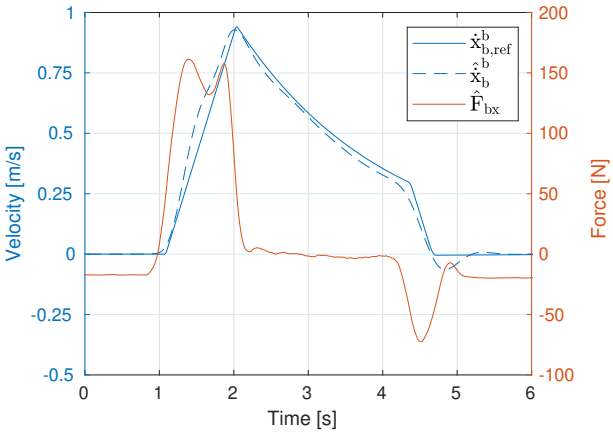

Fig. 18: Observed disturbance (orange), generated velocity setpoint (solid blue) and estimated platform velocity (dashed blue) in the local x-direction of the platform.

Furthermore, the figure shows that a disturbance of about 20 N was observed before the beginning and after the end of the movement, although no user force was exerted on the platform at these moments. As desired, the platform does not react to these observed disturbances as a result of the safety limit of 40 N. Besides, these observed disturbances give an interesting insight about the static friction of the system, in addition to the results described in Section VIII-A. As the velocity and acceleration, as well as their estimates, were zero at these moments, the values of all dynamic parameters in the model have no influence on the observed disturbance. Therefore, the observed disturbance is purely based on the fact that wheel input torques were present without causing a movement. As in reality no user input was applied, this indicates the presence of static friction and its influence on the observed disturbance around zero velocity.

IX. Conclusion and Recommendations for Future Work

In this research, a modular framework has been developed for support of human-induced movements of the ropod platform. Because the compliant control framework is used in combination with a disturbance observer to estimate the user input, the user can exert a force anywhere on the system. The estimated user force is converted to a velocity setpoint via an admittance interface with safety constraints. This setpoint is tracked by the already existing stabilizing velocity controller for the platform.

The modularity has been achieved by developing a modular dynamic model, together with a dynamic parameter identification method that supports this modularity. In this way, a framework is provided in which the wheel configuration of a platform can be changed and multiple collaborating platforms could easily be combined. If rigidly attached to each other, the combination could be seen as one large platform with more wheels. Another possibility for extending the framework is for a situation in which multiple platforms are attached to a load and the load is not placed on top of the ropods, but for instance has its own wheels. Then, the additional kinematic constraints introduced by these wheels will have to be included in the model as well, next to the inertial parameters of the load. This can be done by either giving the required information to the platform, or by finding a method to let the system derive these kinematic constraints and the inertial parameters by itself. However, the experiments executed in this research were restricted to the application of a single ropod platform without a load. A disadvantage of the general and modular dynamic parameter identification method is that is does not provide accurate values for the individual parameters, but only focuses on the accuracy of the model as a whole at the level of the equations of motion of the central component. Therefore, other identification methods might be preferred if the values of the individual parameters would be of interest.

The admittance interface provides a way to let the user experience an interaction with the system as if it has other dynamic properties, so that the movements he induces on the platform require less effort. Due to the limited accuracy of the model and thus the observed disturbance, in combination with the desired safety constraints, the user should now provide a relatively large force before

the system will react. As a consequence, there are cases in which the proposed control strategy would rather require more effort from the user than that the desired movements are supported. However, the experiments have shown that the approach works, and continuation of this research is recommended. If the accuracy of the model and thus the observed user disturbance could be improved further, the limits that are applied to meet the safety constraints could be reduced, so that the amount of effort required from the user could be less. This accuracy can be improved in two ways: by improving the accuracy of the model that is used to estimate the disturbance, or by measuring the user input in another way. It could for instance be measured by a dedicated end-effector instead of by the disturbance observer, which would however have the disadvantage that the user cannot apply his input force anywhere on the system anymore. The application of a combination of both could also be investigated, to use the advantages of both. As the user input is then known due to the end-effector, it is perhaps even possible to identify the dynamic parameters online during the real-time application. Without such a sensor, a separate identification experiment without user input is namely required, as the effect from the user input cannot be distinguished from the platform's own dynamics before the dynamic parameters have been identified.

In any case, it is strongly recommended to further investigate the influence of the small caster offset, in particular in combination with the static friction that is not included in the model yet. Increasing this offset would, according to the hypothesis that followed from the executed experiments and is supported by the developed model of the system, cause a reduction of the required effort from a person to start a movement of the platform in cases in which the wheels are not aligned. Besides, this adaption would help to prevent caster flutter.

Finally, in this research it has been assumed that the system is on a horizontal surface and the influence of gravity in the plane of motion has thus not been modeled. On a sloped surface, this influence would therefore be misinterpreted as a user input and could cause instability of the system. Hence, the inclusion of gravity in the correct direction could be a valuable future addition to the model.

REFERENCES

[1] *Objectives*. (2018). Ropod. http://www.ropod.org/objectives.html

[2] Lopez Martinez, C. A. (2018). *TRL5 prototype of low-level motion controller for joint level and Cartesian level control of smart wheel*.

[3] Macfarlane, G. J., Thomas, E., Papageorgiou, A. C., Croft, P. R., Jayson, M. I. V., & Silman, A. J. (1997). Employment and Physical Work Activities as Predictors of Future Low Back Pain. *Spine*, 22(10), 1143–1149. https://doi.org/10.1097/00007632-199705150-00015

[4] De Groot, P. J. M., Lopez Martinez, C. A., Van de Molengraft, M. J. G., & Bruyninckx, H. P. J. (2019). *Low-cost End-effector and Controller Design for a Compliant Autonomous Mobile Robot*.

[5] Unkel, J.J.E., Lopez Martinez, C. A., Van de Molengraft, M. J. G., & Bruyninckx, H. P. J. (2018). *ROPOD: Force Sensorless Compliant Control for Mobile Robots*.

[6] Browning, R. C., Baker, E. A., Herron, J. A., & Kram, R. (2006). Effects of obesity and sex on the energetic cost and preferred speed of walking. *Journal of Applied Physiology*, 100(2), 390–398. https://doi.org/10.1152/japplphysiol.00767.2005

[7] Schumacher, M., Wojtusch, J., Beckerle, P., & von Stryk, O. (2019). An introductory review of active compliant control. *Robotics and Autonomous Systems*, 119, 185–200. https://doi.org/10.1016/j.robot.2019.06.009

[8] Dietrich, A., Bussmann, K., Petit, F., Kotyczka, P., Ott, C., Lohmann, B., & Albu-Schäffer, A. (2015). Whole-body impedance control of wheeled mobile manipulators. *Autonomous Robots*, 40(3), 505–517. https://doi.org/10.1007/s10514-015-9438-z

[9] Wannasuphoprasit, W., Gillespie, R., Colgate, J., & Peshkin, M. (1997). Cobot control. *Proceedings of International Conference on Robotics and Automation*. https://doi.org/10.1109/robot.1997.606888

[10] Gillespie, R. B., Colgate, J. E., & Peshkin, M. A. (2001). A general framework for cobot control. *IEEE Transactions on Robotics and Automation*, 17(4), 391–401. https://doi.org/10.1109/70.954752

[11] Kyoungchul Kong, & Doyoung Jeon. (2006). Design and control of an exoskeleton for the elderly and patients. *IEEE/ASME Transactions on Mechatronics*, 11(4), 428–432. https://doi.org/10.1109/tmech.2006.878550

[12] Kazerooni, H., Racine, J. L., Lihua Huang, & Steger, R. (2005). On the Control of the Berkeley Lower Extremity Exoskeleton (BLEEX). *Proceedings of the 2005 IEEE International Conference on Robotics and Automation*. https://doi.org/10.1109/robot.2005.1570790

[13] Oh, S., Baek, E., Song, S., Mohammed, S., Jeon, D., & Kong, K. (2015). A generalized control framework of assistive controllers and its application to lower limb exoskeletons. *Robotics and Autonomous Systems*, 73, 68–77. https://doi.org/10.1016/j.robot.2014.10.001

[14] Siciliano, B., Sciavicco, L., Villani, L., & Oriolo, G. (2009). *Robotics: Modelling, Planning and Control*. Springer.

[15] Spong, M. W., Hutchinson, S., & Vidyasagar, M. (2005). *Robot Modeling and Control* (1st ed.). Wiley.

[16] Jin, J., & Gans., N. (2015). Parameter identification for industrial robots with a fast and robust trajectory design approach, *Robotics and Computer-Integrated Manufacturing*, Volume 31, 21-29, ISSN 0736-5845, https://doi.org/10.1016/j.rcim.2014.06.004

[17] Wu, J., Wang, J., & You, Z. (2010). An overview of dynamic parameter identification of robots. *Robotics and Computer-Integrated Manufacturing*, 26(5), 414–419. https://doi.org/10.1016/j.rcim.2010.03.013

[18] Van Dommelen, A.J., W. Houtman, W., & Van de Molengraft, M.J.G. (2020). *Slip Avoidance for Load Hauling AGVs on Unfamiliar Surfaces*.

[19] Skogestad, S., & Postlethwaite, I. (2005). *Multivariable feedback control: analysis and design*. Chichester: John Wiley & Sons, Inc.

[20] Woods, D. L., Wyma, J. M., Yund, E. W., Herron, T. J., & Reed, B. (2015). Factors influencing the latency of simple reaction time. *Frontiers in Human Neuroscience*, 9. https://doi.org/10.3389/fnhum.2015.00131

[21] Caster Concepts, Inc. (2020, February 21). *Causes and Corrections of Caster Flutter*. Caster Concepts. https://www.casterconcepts.com/solutions/ergonomic-casters/causes-and-corrections-of-caster-flutter

APPENDIX A
GEOMETRIC PARAMETER VALUES

In Table I the geometric parameters of the platform used for this research are given. The descriptions of these parameters are supported by the illustrations in Fig. 10, 11 and 12.

TABLE I: Geometric parameter values ropod platform

Parameter	Description	Value [cm]
d_w	Distance between wheels	8.0
s_w	Swivel offset	1.0
Δ_x	SWh center of gravity offset	-0.5
R_w	Wheel radius	5.25
$r^b_{1b/b}$	Location pivot point SWh 1	$[21.0 \;\; 21.0]^\top$
$r^b_{2b/b}$	Location pivot point SWh 2	$[-21.0 \;\; 21.0]^\top$
$r^b_{3b/b}$	Location pivot point SWh 3	$[-21.0 \;\; -21.0]^\top$
$r^b_{4b/b}$	Location pivot point SWh 4	$[21.0 \;\; -21.0]^\top$

APPENDIX B
MATRIX PARAMETRIZATION

The parametrization of a matrix will in this project in particular be applied to the second time derivative of a rotation matrix. A scalar variable q can be parametrized in an affine way with respect to a column q^* in the form $q = a^q_{q^*} q^* + b^q$ where $a^q_{q^*}$ is a row and b^q is a scalar. Similarly, a column of variables q can be parametrized with respect to a column q^* in the form $q = A^q_{q^*} q^* + b^q$ where $A^q_{q^*}$ is a matrix and b^q is a column. However, when parametrizing a matrix of variables Q, another structure should be found (or higher dimensional matrices should be applied). Proposed here is the form $Q = A^Q_{\bar{q}^*} \bar{q}^* + B^Q$ where $A^Q_{\bar{q}^*}$ is a matrix, $\bar{q}^*$ is a matrix and B^Q is a matrix. The main difference is that $\bar{q}^*$ is a non-rectangular block diagonal matrix with columns q^* as blocks on its block-diagonal.

As an example, the parametrization of $\ddot{R}^0_b$ with respect to $\ddot{q}^0_b$ will be shown here:

$$\begin{aligned}
\ddot{R}^0_b &= \begin{bmatrix} -\ddot{\theta}_b s_{\theta_b} - \dot{\theta}_b^2 c_{\theta_b} & -\ddot{\theta}_b c_{\theta_b} + \dot{\theta}_b^2 s_{\theta_b} \\ \ddot{\theta}_b c_{\theta_b} - \dot{\theta}_b^2 s_{\theta_b} & -\ddot{\theta}_b s_{\theta_b} - \dot{\theta}_b^2 c_{\theta_b} \end{bmatrix} \\
&= \begin{bmatrix} -\ddot{\theta}_b s_{\theta_b} & -\ddot{\theta}_b c_{\theta_b} \\ \ddot{\theta}_b c_{\theta_b} & -\ddot{\theta}_b s_{\theta_b} \end{bmatrix} + \underbrace{\begin{bmatrix} -\dot{\theta}_b^2 c_{\theta_b} & \dot{\theta}_b^2 s_{\theta_b} \\ \dot{\theta}_b^2 s_{\theta_b} & -\dot{\theta}_b^2 c_{\theta_b} \end{bmatrix}}_{B^{\ddot{R}^0_b}} \\
&= \underbrace{\begin{bmatrix} 0 & 0 & -s_{\theta_b} & 0 & 0 & -c_{\theta_b} \\ 0 & 0 & c_{\theta_b} & 0 & 0 & -s_{\theta_b} \end{bmatrix}}_{A^{\ddot{R}^0_b}_{\ddot{\bar{q}}^0_b}} \underbrace{\begin{bmatrix} \ddot{x}^0_b & 0 \\ \ddot{y}^0_b & 0 \\ \ddot{\theta}_b & 0 \\ 0 & \ddot{x}^0_b \\ 0 & \ddot{y}^0_b \\ 0 & \ddot{\theta}_b \end{bmatrix}}_{\ddot{\bar{q}}^0_b} + B^{\ddot{R}^0_b}
\end{aligned} \tag{43}$$

For the second order derivatives of rotation matrices that have a dependency on other second order time derivatives than the ones contained in $\ddot{q}^0_b$, some additional steps are required to find the expressions for the parametrization. As can be seen in the expression for $\ddot{R}^0_i$ used in (9c), there is a direct dependency on $\ddot{\theta}_i$. Starting from that expression, we can again parametrize with respect to (only) $\ddot{q}^0_b$ by first restructuring it to:

$$\begin{aligned}
\ddot{R}^0_i &= \begin{bmatrix} -\ddot{\theta}_i s_{\theta_i} - \dot{\theta}_i^2 c_{\theta_i} & -\ddot{\theta}_i c_{\theta_i} + \dot{\theta}_i^2 s_{\theta_i} \\ \ddot{\theta}_i c_{\theta_i} - \dot{\theta}_i^2 s_{\theta_i} & -\ddot{\theta}_i s_{\theta_i} - \dot{\theta}_i^2 c_{\theta_i} \end{bmatrix} \\
&= \underbrace{\begin{bmatrix} -s_{\theta_i} & -c_{\theta_i} \\ c_{\theta_i} & -s_{\theta_i} \end{bmatrix}}_{A^{\ddot{R}^0_i}_{\ddot{\theta}_i}} \begin{bmatrix} \ddot{\theta}_i & 0 \\ 0 & \ddot{\theta}_i \end{bmatrix} + \underbrace{\begin{bmatrix} -\dot{\theta}_i^2 c_{\theta_i} & \dot{\theta}_i^2 s_{\theta_i} \\ -\dot{\theta}_i^2 s_{\theta_i} & -\dot{\theta}_i^2 c_{\theta_i} \end{bmatrix}}_{B^{\ddot{R}^0_i}_{\ddot{\theta}_i}}
\end{aligned} \tag{44}$$

And since $\ddot{\theta}_i = a^{\ddot{\theta}_i}_{\ddot{q}^0_b} \ddot{q}^0_b + b^{\ddot{\theta}_i}$, we can now write for each element (k,l) of $\ddot{R}^0_i$:

$$\begin{aligned}
\ddot{R}^0_{i,kl} &= A^{\ddot{R}^0_i}_{\ddot{\theta}_i,kl} \ddot{\theta}_i + B^{\ddot{R}^0_i}_{\ddot{\theta}_i,kl} \\
&= A^{\ddot{R}^0_i}_{\ddot{\theta}_i,kl} \left(a^{\ddot{\theta}_i}_{\ddot{q}^0_b} \ddot{q}^0_b + b^{\ddot{\theta}_i} \right) + B^{\ddot{R}^0_i}_{\ddot{\theta}_i,kl} \\
&= \underbrace{A^{\ddot{R}^0_i}_{\ddot{\theta}_i,kl} a^{\ddot{\theta}_i}_{\ddot{q}^0_b}}_{A^{\ddot{R}^0_i}_{\ddot{\bar{q}}^0_b,kl}} \ddot{q}^0_b + \underbrace{A^{\ddot{R}^0_i}_{\ddot{\theta}_i,kl} b^{\ddot{\theta}_i} + B^{\ddot{R}^0_i}_{\ddot{\theta}_i,kl}}_{B^{\ddot{R}^0_i}_{kl}}
\end{aligned} \tag{45}$$

So that now the $B^{\ddot{R}^0_i}_{kl}$ is element (k,l) of $B^{\ddot{R}^0_i}$ and $A^{\ddot{R}^0_i}_{\ddot{q}^0_b,kl}$ are the 1×3 block elements (k,l) of $A^{\ddot{R}^0_i}_{\ddot{\bar{q}}^0_b}$ that are used to parametrize $\ddot{R}^0_i$ directly with respect to $\ddot{q}^0_b$ in a similar structure to the parametrization of $\ddot{R}^0_b$:

$$\ddot{R}^0_i = A^{\ddot{R}^0_i}_{\ddot{\bar{q}}^0_b} \ddot{\bar{q}}^0_b + B^{\ddot{R}^0_i} \tag{46}$$

For the model described in this research, these second order time derivatives of rotation matrices are always post-multiplied by a column that contains constant values (and therefore do not have to be parametrized). In general this column will have the form $r = \begin{bmatrix} r_x & r_y \end{bmatrix}^\top$. By introducing an extended matrix version $\bar{r}$ of this column, the parametrization of the two factors can be combined. This extended matrix version is:

$$\bar{r} = \begin{bmatrix} r_x & 0 & 0 \\ 0 & r_x & 0 \\ 0 & 0 & r_x \\ r_y & 0 & 0 \\ 0 & r_y & 0 \\ 0 & 0 & r_y \end{bmatrix} \tag{47}$$

Applying this to an example based on (5c), in which matrix $\ddot{R}_b^0$ is post-multiplied by $r_{ib/b}^b$, yields:

$$\begin{aligned} \ddot{R}_b^0 r_{ib/b}^b &= \left(A_{\bar{q}_b^0}^{\ddot{R}_b^0} \underbrace{\begin{bmatrix} \ddot{x}_b^0 & 0 \\ \ddot{y}_b^0 & 0 \\ \ddot{\theta}_b & 0 \\ 0 & \ddot{x}_b^0 \\ 0 & \ddot{y}_b^0 \\ 0 & \ddot{\theta}_b \end{bmatrix}}_{\bar{q}_b^0} + B^{\ddot{R}_b^0} \right) \underbrace{\begin{bmatrix} x_{ib/b}^b \\ y_{ib/b}^b \end{bmatrix}}_{r_{ib/b}^b} \\ &= A_{\bar{q}_b^0}^{\ddot{R}_b^0} \begin{bmatrix} \ddot{x}_b^0 x_{ib/b}^b \\ \ddot{y}_b^0 x_{ib/b}^b \\ \ddot{\theta}_b x_{ib/b}^b \\ \ddot{x}_b^0 y_{ib/b}^b \\ \ddot{y}_b^0 y_{ib/b}^b \\ \ddot{\theta}_b y_{ib/b}^b \end{bmatrix} + B^{\ddot{R}_b^0} r_{ib/b}^b \\ &= A_{\bar{q}_b^0}^{\ddot{R}_b^0} \underbrace{\begin{bmatrix} x_{ib/b}^b & 0 & 0 \\ 0 & x_{ib/b}^b & 0 \\ 0 & 0 & x_{ib/b}^b \\ y_{ib/b}^b & 0 & 0 \\ 0 & y_{ib/b}^b & 0 \\ 0 & 0 & y_{ib/b}^b \end{bmatrix}}_{\bar{r}_{ib/b}^b} \underbrace{\begin{bmatrix} \ddot{x}_b^0 \\ \ddot{y}_b^0 \\ \ddot{\theta}_b \end{bmatrix}}_{\ddot{q}_b^0} + B^{\ddot{R}_b^0} r_{ib/b}^b \\ &= \underbrace{A_{\bar{q}_b^0}^{\ddot{R}_b^0} \bar{r}_{ib/b}^b}_{A_{\ddot{q}_b^0}^{\ddot{R}_b^0 r_{ib/b}^b}} \ddot{q}_b^0 + \underbrace{B^{\ddot{R}_b^0} r_{ib/b}^b}_{b^{\ddot{R}_b^0 r_{ib/b}^b}} \end{aligned} \tag{48}$$

APPENDIX C
PROOF OF INVERTIBILITY OF THE MASS MATRIX

In order to be able to use the forward dynamics of the direct equations of motion, given in (33), matrix M_{dir} should be invertible. The kinetic energy of the system as a whole could be calculated by $T = \frac{1}{2}\dot{q}_b^{0\top} M_{dir} \dot{q}_b^0$, which should physically be larger than zero for any nonzero $\dot{q}_b^0$ (because the movement of the base itself has a positive contribution and the additional SWhs can never have a negative contribution), which means that M_{dir} would be positive definite and thus invertible. However, the proof can also be given mathematically. Matrix M_{dir} is invertible if and only if $\det(M_{dir}) \neq 0$. A sufficient condition for that is when M_{dir} is positive definite. Proving this positive definiteness can be done by rewriting the expression for M_{dir} from (32):

$$\begin{aligned} M_{dir} &= M_b - \sum_{i=1}^{n} B_{F_{ixy}} A_{\ddot{q}_b^0}^{F_{ixy}} \\ &= M_b + \sum_{i=1}^{n} \underbrace{-B_{F_{ixy}} A_{\ddot{q}_b^0}^{F_{ixy}}}_{M_{i,add}} \end{aligned} \tag{49}$$

Now, a sufficient condition for M_{dir} being positive definite is when M_b is positive definite and $M_{i,add}$ is positive (semi-)definite for any $i \in \{1, ..., n\}$. Proving that M_b is positive definite is straightforward, as it is the mass matrix of the base only: the eigenvalues are m_b (twice) and $J_{zz,b}$, which are all positive. Matrix $M_{i,add}$ is positive (semi-)definite when all its leading principal minors are positive (or zero), i.e. the determinants of its upper-left $k \times k$ sub-matrix is positive (or zero) for any $k \in \{1, 2, 3\}$, as $M_{i,add}$ is a 3×3 matrix. The expressions for those leading principal minors were calculated using the Matlab Symbolic Toolbox. The first leading principal minor is equal to element $(1, 1)$ of $M_{i,add}$:

$$\begin{aligned} M_{i,add,11} = \frac{s_{\theta_i}^2}{2R_w^2 s_w^2} \big(&2J_{zz,wh} R_w^2 + J_{rot,w} d_w^2 + 4J_{rot,w} s_w^2 \\ &+ 2\Delta_x^2 R_w^2 m_{wh} + 2R_w^2 m_{wh} s_w^2 \big) \end{aligned} \tag{50}$$

which is only equal to zero when $\sin(\theta_i) = 0$, so when $\theta_i = k\pi, k \in \mathbb{Z}$, and positive otherwise, because m_{wh}, $J_{zz,wh}$ and $J_{rot,w}$ are positive and R_w, s_w and d_w are nonzero.

The second leading principal minor is the determinant of the upper-left 2×2 sub-matrix of $M_{i,add}$:

$$\begin{aligned} \det(M_{i,add,\{1,2\}\{1,2\}}) = &\frac{m_{wh} R_w^2 + 2J_{rot,w}}{2R_w^4 s_w^2} \big(J_{rot,w} d_w^2 \\ &+ 2m_{wh} \Delta_x^2 R_w^2 + 2J_{zz,wh} R_w^2 \big) \end{aligned} \tag{51}$$

which is also positive because the parameters m_{wh}, $J_{zz,wh}$ and $J_{rot,w}$ are positive and R_w, s_w and d_w are nonzero.

The third and last leading principal minor is the determinant of $M_{i,add}$, which appears to be equal to 0, regardless of the values of the dynamic and geometric parameters. This result is logical since $M_{i,add}$ is the product of $B_{F_{ixy}}$ and $A_{\dot{q}_b^0}^{F_{ixy}}$ (with a minus sign), which are 3×2 and 2×3 matrices respectively and can thus never have a rank higher than 2. The product of two matrices can never have a rank that is higher than the minimum rank of the matrices it consists of. So $M_{i,add}$ can never have a rank higher than 2, thus it is not full rank and has a determinant equal to 0.

In summary, all leading principal minors of $M_{i,add}$ are larger than or equal to 0 (with the sufficient condition that m_{wh}, $J_{zz,wh}$ and $J_{rot,w}$ are positive and R_w, s_w and d_w are nonzero), so $M_{i,add}$ is positive semi-definite for any $i \in \{1, ..., n\}$. Hence, M_{dir} is positive definite and therefore invertible.

APPENDIX D
FRICTION

In order to indicate whether friction plays a significant role in the platform dynamics and should thus be included in the model, the following experiment has been executed. The platform follows a trajectory at different constant velocities in a straight line, so that the wheels remain aligned with the platform and the inertial effects are limited. During 2.0 seconds of driving at such a constant velocity, the total wheel input torques are calculated and then averaged over time. This has been repeated four times for all different velocities and the results are shown in Fig. 19. The linear fit with the least squares error trough the data points yields:

$$\sum \tau = 1.614 + 0.067\dot{x}_b^0 \tag{52}$$

with a remaining standard deviation of 0.051 Nm for the error. Given that the wheel radius R_w is 0.0525 m, the total torque corresponds to a force of over 30 N at platform level, which is significant and therefore a reason for the inclusion of friction in the model.

The two movements for which friction is assumed to play the most significant role are the rolling movement of an individual wheel and the pivot rotation of a SWh with respect to the platform base. These sources of fiction will both be discussed in this appendix, including an explanation of how they fit in the structure of the modular dynamic model and how the friction coefficients are included in the dynamic parameter identification method.

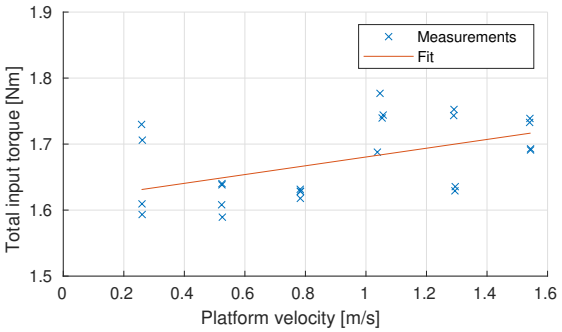

Fig. 19: Total input torque required for driving at different constant velocities

A. Roll Friction

The friction for the rolling movement of an individual wheel occurs due to interaction with the ground and internal friction (motor, axis). As the dynamics in vertical direction are not considered and there is an assumption of no slip, the friction can be described by a torque about the wheel axis only. Taking a contribution of the friction force in horizontal direction into account would namely be unnecessary, as the computed reaction force in this direction would be corrected for it and the total effect would remain equal. The proposed friction model is chosen based on the shape of the results in Fig. 19 and is:

$$\tau_{fw,iw} = f_{wv}\dot{\phi}_{iw} + f_{wc}\tanh(\alpha\dot{\phi}_{iw}) \tag{53}$$

in which f_{wv} is the viscous friction coefficient, f_{wc} is the Coulomb friction coefficient. The Sigmoid function $\tanh(\alpha\dot{\phi}_{iw})$ instead of $\text{sign}(\dot{\phi}_{iw})$ and the absence of the often used Stribeck effect are chosen to avoid discontinuities, despite the fact that this is in fact the opposite of what would be desired in order to model static friction. The value for α was chosen to be 10, based on how close the typical estimated velocities are to zero at the moment the platform is not moving in practice.

The advantage of taking this approach is that this friction can be included in the dynamic model by simply adding the wheel friction $\tau_{fw,iw}$ at any place where a wheel input τ_{iw} is used. For example, (17) becomes:

$$\ddot{\phi}_{iw} = \frac{1}{J_{rot,w}}\left(\tau_{iw} + \tau_{fw,iw} - F_{iw}R_w\right) \tag{54}$$

and on the highest level, the direct equations of motion become:

$$M_{dir}\ddot{q}_b^0 = B_{F_p}F_p + B_\tau\left(\tau + \tau_{fw}\right) + b_{dir} \tag{55}$$

Another way to write it could be by incorporating $B_\tau \tau_{fw}$ in b_{dir}. However, by letting it be a separate term, it is more straightforward to directly include the friction coefficients for the dynamic parameter identification, as will be shown in Appendix D-C. The column of wheel friction torques can be written as

$$\tau_{fw} = \begin{bmatrix} \tau_{fw,1L} \\ \tau_{fw,1R} \\ \tau_{fw,2L} \\ \vdots \\ \tau_{fw,nR} \end{bmatrix} = \begin{bmatrix} f_{wv}\dot{\phi}_{1L} + f_{wc}\tanh(\alpha\dot{\phi}_{1L}) \\ f_{wv}\dot{\phi}_{1R} + f_{wc}\tanh(\alpha\dot{\phi}_{1R}) \\ f_{wv}\dot{\phi}_{2L} + f_{wc}\tanh(\alpha\dot{\phi}_{2L}) \\ \vdots \\ f_{wv}\dot{\phi}_{nR} + f_{wc}\tanh(\alpha\dot{\phi}_{nR}) \end{bmatrix}$$
$$= \underbrace{\begin{bmatrix} \dot{\phi}_{1L} & \tanh(\alpha\dot{\phi}_{1L}) \\ \dot{\phi}_{1R} & \tanh(\alpha\dot{\phi}_{1R}) \\ \dot{\phi}_{2L} & \tanh(\alpha\dot{\phi}_{2L}) \\ \vdots & \vdots \\ \dot{\phi}_{nR} & \tanh(\alpha\dot{\phi}_{nR}) \end{bmatrix}}_{A_{fw}} \underbrace{\begin{bmatrix} f_{wv} \\ f_{wc} \end{bmatrix}}_{f_w} \tag{56}$$

Note that it is assumed that the friction coefficients have the same value for each wheel. If it is desired to have different coefficient values per individual wheel, the structure becomes:

$$\tau_{fw} = \begin{bmatrix} \tau_{fw,1L} \\ \tau_{fw,1R} \\ \tau_{fw,2L} \\ \vdots \\ \tau_{fw,nR} \end{bmatrix} = \begin{bmatrix} f_{wv,1L}\dot{\phi}_{1L} + f_{wc,1L}\tanh(\alpha\dot{\phi}_{1L}) \\ f_{wv,1R}\dot{\phi}_{1R} + f_{wc,1R}\tanh(\alpha\dot{\phi}_{1R}) \\ f_{wv,2L}\dot{\phi}_{2L} + f_{wc,2L}\tanh(\alpha\dot{\phi}_{2L}) \\ \vdots \\ f_{wv,nR}\dot{\phi}_{nR} + f_{wc,nR}\tanh(\alpha\dot{\phi}_{nR}) \end{bmatrix}$$
$$= \underbrace{\begin{bmatrix} A_{fw,1L} & 0_{1\times2} & 0_{1\times2} & \cdots & 0_{1\times2} \\ 0_{1\times2} & A_{fw,1R} & 0_{1\times2} & \cdots & 0_{1\times2} \\ 0_{1\times2} & 0_{1\times2} & A_{fw,2L} & \cdots & 0_{1\times2} \\ \vdots & \vdots & \vdots & \ddots & \vdots \\ 0_{1\times2} & 0_{1\times2} & 0_{1\times2} & \cdots & A_{fw,nR} \end{bmatrix}}_{A_{fw}} \underbrace{\begin{bmatrix} f_{wv,1L} \\ f_{wc,1L} \\ f_{wv,1R} \\ f_{wc,1R} \\ f_{wv,2L} \\ f_{wc,2L} \\ \vdots \\ f_{wv,nR} \\ f_{wc,nR} \end{bmatrix}}_{f_w} \tag{57}$$

in which $A_{fw,iw} = \begin{bmatrix} \dot{\phi}_{iw} & \tanh(\alpha\dot{\phi}_{iw}) \end{bmatrix}$ for $i \in \{1, ..., n\}$ and $w \in \{L, R\}$.

B. Pivot Friction

The individual pivot friction torques $\tau_{fp,i}$ are dependent on the difference $\dot{\delta}_i$ between the angular velocities of the platform base and SWh i. The proposed friction model is similar to the one for the roll friction:

$$\tau_{fp,i} = f_{pv}\dot{\delta}_i + f_{pc}\tanh(\alpha\dot{\delta}_i) \tag{58}$$

and hence we can write:

$$\tau_{fp} = \underbrace{\begin{bmatrix} \dot{\delta}_1 & \tanh(\alpha\dot{\delta}_1) \\ \dot{\delta}_2 & \tanh(\alpha\dot{\delta}_2) \\ \vdots & \vdots \\ \dot{\delta}_n & \tanh(\alpha\dot{\delta}_n) \end{bmatrix}}_{A_{fp}} \underbrace{\begin{bmatrix} f_{pv} \\ f_{pc} \end{bmatrix}}_{f_p} \tag{59}$$

when the friction coefficients have the same value for each pivot. If it is desired to have different coefficient values per individual pivot, the structure becomes:

$$\tau_{fp} = \underbrace{\begin{bmatrix} A_{fp,1} & 0_{2\times1} & \cdots & 0_{2\times1} \\ 0_{2\times1} & A_{fp,2} & \cdots & 0_{2\times1} \\ \vdots & \vdots & \ddots & 0_{2\times1} \\ 0_{2\times1} & 0_{2\times1} & \cdots & A_{fp,n} \end{bmatrix}}_{A_{fp}} \underbrace{\begin{bmatrix} f_{pv,1} \\ f_{pc,1} \\ f_{pv,2} \\ f_{pc,2} \\ \vdots \\ f_{pv,n} \\ f_{pc,n} \end{bmatrix}}_{f_p} \tag{60}$$

in which $A_{fp,i} = \begin{bmatrix} \dot{\delta}_i & \tanh(\alpha\dot{\delta}_i) \end{bmatrix}$ for $i \in \{1, ..., n\}$.

As the pivot friction is an interaction torque between the platform base and a SWh, its contribution should be considered in the dynamics of both components. For the platform base, the added terms will be the friction torques that effect the angular acceleration, which can be added to the direct equations of motion in a straightforward way:

$$M_b\ddot{q}_b^0 = B_{F_b}F_b + \sum_{i=1}^{n} B_{F_{ixy}}F_{ixy} + \sum_{i=1}^{n} \begin{bmatrix} 0 \\ 0 \\ \tau_{fp,i} \end{bmatrix} \tag{61}$$

However, this friction will also effect the wheel hub dynamics, and hence change the expression for the interaction forces, influencing the direct equations of motion via this way as well. As the friction torque acting on the wheel hub can be seen as a reaction torque for the friction that acts on the platform base at the corresponding pivot point, its magnitude is equal and its direction is opposite. Therefore, (18) becomes:

$$M_{wh}\ddot{q}_{icm}^0 = A_{iwh}\begin{bmatrix} F_{ix} \\ F_{iy} \\ F_{iS} \end{bmatrix} + A_{iwh2}F_{iLR} - \begin{bmatrix} 0 \\ 0 \\ \tau_{fp,i} \end{bmatrix} \tag{62}$$

and (22) accordingly becomes:

$$\begin{bmatrix} F_{ix} \\ F_{iy} \\ F_{iS} \end{bmatrix} = A_{\ddot{q}_b^0}^{F_{ixyS}}\ddot{q}_b^0 + A_{\tau_i}^{F_{ixyS}}\tau_i + b^{F_{ixyS}} + A_{iwh}^{-1}\begin{bmatrix} 0 \\ 0 \\ \tau_{fp,i} \end{bmatrix} \tag{63}$$

Considering these contributions on both components, the new direct equations of motion (an extended version of (32)) in which the effect of the pivot friction is isolated can be derived:

$$
\begin{aligned}
M_b\ddot{q}_b^0 &= B_{F_b}F_b + \sum_{i=1}^{n} B_{F_{ixy}} \underbrace{\left(A_{\ddot{q}_b^0}^{F_{ixy}}\ddot{q}_b^0 + A_{\tau_i}^{F_{ixy}}\tau_i + b^{F_{ixy}} + \begin{bmatrix}1&0&0\\0&1&0\end{bmatrix} A_{iwh}^{-1} \begin{bmatrix}0\\0\\\tau_{fp,i}\end{bmatrix} \right)}_{F_{ixy}} + \sum_{i=1}^{n} \begin{bmatrix}0\\0\\\tau_{fp,i}\end{bmatrix} \\
\underbrace{\left(M_b - \sum_{i=1}^{n} B_{F_{ixy}} A_{\ddot{q}_b^0}^{F_{ixy}} \right)}_{M_{dir}} \ddot{q}_b^0 &= B_{F_b}F_b + \sum_{i=1}^{n} \underbrace{B_{F_{ixy}} A_{\tau_i}^{F_{ixy}}}_{B_{\tau_i}} \tau_i + \underbrace{\sum_{i=1}^{n} B_{F_{ixy}} b^{F_{ixy}}}_{b_{dir}} \\
&\quad + \sum_{i=1}^{n} \underbrace{\left(I_{3\times3} + B_{F_{ixy}} \begin{bmatrix}1&0&0\\0&1&0\end{bmatrix} A_{iwh}^{-1} \right) \begin{bmatrix}0\\0\\1\end{bmatrix}}_{B_{\tau_{fp,i}}} \tau_{fp,i} \\
M_{dir}\ddot{q}_b^0 &= B_{F_b}F_b + \underbrace{\begin{bmatrix} B_{\tau_1} & B_{\tau_2} & \cdots & B_{\tau_n} \end{bmatrix}}_{B_\tau} \underbrace{\begin{bmatrix}\tau_1\\\tau_2\\\vdots\\\tau_n\end{bmatrix}}_{\tau} + b_{dir} + \underbrace{\begin{bmatrix} B_{\tau_{fp,1}} & B_{\tau_{fp,2}} & \cdots & B_{\tau_{fp,n}} \end{bmatrix}}_{B_{\tau_{fp}}} \underbrace{\begin{bmatrix}\tau_{fp,1}\\\tau_{fp,2}\\\vdots\\\tau_{fp,n}\end{bmatrix}}_{\tau_{fp}}
\end{aligned}
\tag{64}
$$

In conclusion, together with the roll friction, the direct equations of motion can now be written as:

$$M_{dir}\ddot{q}_b^0 = B_{F_b}F_b + B_\tau(\tau + \tau_{fw}) + B_{\tau_{fp}}\tau_{fp} + b_{dir} \tag{65}$$

C. Parameter Identification

The friction coefficients can depend on for instance the weight of the platform and the properties of the floor. These dependencies are implicitly taken into account by doing the the parameter identification under the same circumstances as in which the model is applied.

In order to include the friction coefficients in the dynamic parameter identification discussed in Section VI, the same approach as applied in (35) can be followed. The equations of motion including friction are rewritten as follows:

$$
\begin{aligned}
M_{dir}\ddot{q}_b^0 &= \underbrace{B_{F_p}F_p + B_\tau\tau}_{b_{ID}} + B_\tau\tau_{fw} + B_{\tau_{fp}}\tau_{fp} + b_{dir} \\
M_{dir}\ddot{q}_b^0 - b_{dir} &= b_{ID} + B_\tau \underbrace{A_{fw}f_w}_{\tau_{fw}} + B_{\tau_{fp}} \underbrace{A_{fp}f_p}_{\tau_{fp}} \\
A_{ID}\underline{m} &= b_{ID} + B_\tau A_{fw}f_w + B_{\tau_{fp}}A_{fp}f_p \\
\underbrace{\begin{bmatrix} A_{ID} & -B_\tau A_{fw} & -B_{\tau_{fp}}A_{fp} \end{bmatrix}}_{A_{ID,ext}} \underbrace{\begin{bmatrix}\underline{m}\\f_w\\f_p\end{bmatrix}}_{\underline{m}_{ext}} &= b_{ID}
\end{aligned}
\tag{66}
$$

Now, with the extended system identification matrix $A_{ID,ext}$ and the extended vector of dynamic parameters $\underline{m}_{ext}$ instead of A_{ID} and $\underline{m}$, the resulting system of equations has the same structure as for the model without friction.

APPENDIX E
IDENTIFIED DYNAMIC PARAMETER VALUES

In Table II the values of dynamic parameters as identified using the approach from Section VI are given for the platform used for this research. The descriptions of these parameters are supported by explanation of the dynamic model in Section V and the explanation of the addition of friction to the model in Appendix D. The values for m_b and m_{wh} for the model fit with these fixed mass values were determined using a scale. The mass of the platform as a whole including its four SWhs is 51.9 kg. The mass m_{wh} of a SWh is 4.2 kg. Hence, the calculated mass m_b of the platform base without the four SWhs is 35.1 kg.

TABLE II: Identified dynamic parameter values ropod platform

Parameter	**Description**	**Identified Value**		**Unit**
		Standard Fit	**Fixed Masses**	
m_b	Platform base mass	-20.4100	35.1000	kg
$J_{zz,b}$	Platform base moment of inertia about vertical axis	-3.8987	3.8145	kgm^2
m_{wh}	SWh mass	-87.5331	4.2000	kg
$J_{zz,wh}$	SWh moment of inertia about vertical axis	-0.1661	-0.0026	kgm^2
$J_{rot,w}$	Individual wheel moment of inertia about axle	0.1559	0.0105	kgm^2
$f_{wv,1L}$	Viscous friction coefficient SWh 1 left wheel	0.0370	0.0529	Nms/rad
$f_{wc,1L}$	Coulomb friction coefficient SWh 1 left wheel	-0.3589	-0.3663	Nm
$f_{wv,1R}$	Viscous friction coefficient SWh 1 right wheel	0.0488	0.0556	Nms/rad
$f_{wc,1R}$	Coulomb friction coefficient SWh 1 right wheel	-0.3001	-0.3326	Nm
$f_{wv,2L}$	Viscous friction coefficient SWh 2 left wheel	-0.0301	-0.0296	Nms/rad
$f_{wc,2L}$	Coulomb friction coefficient SWh 2 left wheel	-0.1792	-0.2598	Nm
$f_{wv,2R}$	Viscous friction coefficient SWh 2 right wheel	-0.0490	-0.0562	Nms/rad
$f_{wc,2R}$	Coulomb friction coefficient SWh 2 right wheel	-0.1174	-0.1716	Nm
$f_{wv,3L}$	Viscous friction coefficient SWh 3 left wheel	0.0141	-0.0186	Nms/rad
$f_{wc,3L}$	Coulomb friction coefficient SWh 3 left wheel	-0.0284	0.0411	Nm
$f_{wv,3R}$	Viscous friction coefficient SWh 3 right wheel	0.0296	-0.0005	Nms/rad
$f_{wc,3R}$	Coulomb friction coefficient SWh 3 right wheel	-0.0617	0.0462	Nm
$f_{wv,4L}$	Viscous friction coefficient SWh 4 left wheel	-0.0251	-0.0144	Nms/rad
$f_{wc,4L}$	Coulomb friction coefficient SWh 4 left wheel	-0.2487	-0.1328	Nm
$f_{wv,4R}$	Viscous friction coefficient SWh 4 right wheel	-0.0340	-0.0087	Nms/rad
$f_{wc,4R}$	Coulomb friction coefficient SWh 4 right wheel	-0.3098	-0.2348	Nm
$f_{pv,1}$	Viscous friction coefficient SWh 1 pivot	0.1136	0.1783	Nms/rad
$f_{pc,1}$	Coulomb friction coefficient SWh 1 pivot	0.0146	0.0279	Nm
$f_{pv,2}$	Viscous friction coefficient SWh 2 pivot	0.1368	0.2110	Nms/rad
$f_{pc,2}$	Coulomb friction coefficient SWh 2 pivot	0.0338	0.0345	Nm
$f_{pv,3}$	Viscous friction coefficient SWh 3 pivot	0.1663	0.2177	Nms/rad
$f_{pc,3}$	Coulomb friction coefficient SWh 3 pivot	0.0051	0.0080	Nm
$f_{pv,4}$	Viscous friction coefficient SWh 4 pivot	0.1431	0.2366	Nms/rad
$f_{pc,4}$	Coulomb friction coefficient SWh 4 pivot	0.0448	0.0383	Nm

Technische Universiteit
Eindhoven
University of Technology

Declaration concerning the TU/e Code of Scientific Conduct for the Master's thesis

I have read the TU/e Code of Scientific Conduct[i].

I hereby declare that my Master's thesis has been carried out in accordance with the rules of the TU/e Code of Scientific Conduct

Date

08-06-2021

Name

Ruben Beumer

ID-number

0967254

Signature

R.M. Beumer

Submit the signed declaration to the student administration of your department.

[i] See: http://www.tue.nl/en/university/about-the-university/integrity/scientific-integrity/
The Netherlands Code of Conduct for Academic Practice of the VSNU can be found here also.
More information about scientific integrity is published on the websites of TU/e and VSNU